SURFACE-EXOSPHERE-MAGNETOSPHERE SYSTEM OF MERCURY

A. MILILLO[1], P. WURZ[2], S. ORSINI[1], D. DELCOURT[3], E. KALLIO[4], R. M. KILLEN[5], H. LAMMER[6], S. MASSETTI[1], A. MURA[1], S. BARABASH[7], G. CREMONESE[8], I. A. DAGLIS[9], E. DE ANGELIS[1], A. M. DI LELLIS[10], S. LIVI[11], V. MANGANO[1,12] and K. TORKAR[6]

[1]*Istituto di Fisica dello Spazio Interplanetario-CNR, Rome, Italy*
[2]*Physics Institute, University of Bern, Sidlerstr. 5, CH-3012 Bern, Switzerland*
[3]*CETP-CNRS, Saint-Maur des Fossés, France*
[4]*Finnish Meteorological Institute, Geophysical Research, Helsinki, Finland*
[5]*Department for Astronomy, University of Maryland, College Park, MD 20742, U.S.A.*
[6]*Space Research Institute, Austrian Academy of Sciences, Schmiedlstr. 6, A-8042 Graz, Austria*
[7]*IRF, Kiruna, Sweden*
[8]*Osservatorio Astronomico-INAF, Padova, Italy*
[9]*Institute for Space Applications and Remote Sensing, NOA, Athens, Greece*
[10]*AMDL s.r.l., Rome, Italy*
[11]*The Johns Hopkins University, Applied Physics Laboratory, Laurel, MD 20723, U.S.A.*
[12]*CISAS, Universita' di Padova, Italy*

Abstract. Mercury is a poorly known planet, since the only space-based information comes from the three fly-bys performed in 1974 by the Mariner 10 spacecraft. Ground-based observations also provided some interesting results, but they are particularly difficult to obtain due to the planet's proximity to the Sun. Nevertheless, the fact that the planet's orbit is so close to the Sun makes Mercury a particularly interesting subject for extreme environmental conditions. Among a number of crucial scientific topics to be addressed, Mercury's exosphere, its interaction with the solar wind and its origin from the surface of the planet, can provide important clues about planetary evolution. In fact, the Hermean exosphere is continuously eroded and refilled by these interactions, so that it would be more proper to consider the Hermean environment as a single, unified system – surface-exosphere-magnetosphere. These three parts are indeed strongly linked to each other. In recent years, the two missions scheduled to explore the iron planet, the NASA MESSENGER mission (launched in March 2004) and the ESA cornerstone mission (jointly with JAXA) BepiColombo (to be launched in 2012), have stimulated new interest in the many unresolved mysteries related to it. New ground-based observations, made possible by new technologies, have been obtained, and new simulation studies have been performed. In this paper some old as well as the very latest observations and studies related to the surface-exosphere-magnetosphere system are reviewed, outlining the investigations achievable by the planned space-based observations. This review intends to support the studies, in preparation of future data, and the definition of specific instrumentation.

Keywords: Mercury exosphere, magnetosphere and surface, solar wind-planet interaction

Space Science Reviews (2005) 117: 397–443
DOI: 10.1007/s11214-005-3593-z

1. Introduction: The Planet Mercury

1.1. Orbital Parameters and Physical Properties

Mercury is the closest planet to the Sun. The mean distance of its orbit is 0.387 AU, the orbital period is 87.969 terrestrial days, and the orbit is highly eccentric $e = 0.205$ (only Pluto's eccentricity is smaller). The spin axis of Mercury is almost perpendicular to the orbital plane. The sidereal day is 58.785 Earth's days, exactly 2/3 of the orbital period. The surface temperature ranges from 700 K in the perihelion subsolar point to 90 K in the aphelion midnight point, giving a large thermal excursion of more than 600 K. The planet radius is $R_M = 2440$ km (2.6 times smaller than that of the Earth). The uncompressed density $= 5.3$ g/cm^3 is the highest of the Solar system bodies (see review by Lewis, 1988) and is attributed to its large iron core. The theoretical estimates of the density of Mercury are below the observed value, even if the same model fits remarkably well, the densities of all the other bodies of the Solar system, including the giant planets and their satellites (Strom, 1984); hence, it is likely that this planet has had a peculiar evolutionary history.

Mariner 10, which provided the first and only close-up observations of Mercury, reported no observational evidence of a proper atmosphere, however, a faint exosphere is present around the planet (Broadfoot *et al*., 1976).

The Mariner 10 fly-bys revealed, unexpectedly, the existence of an internal magnetic field (Ness *et al*., 1975, 1976). Although the magnetic field estimation has large uncertainties due to the difficulties in disentangling the internal and external magnetic field components (Connerney and Ness, 1988), the equivalent magnetic dipole moment could be estimated between 200 and 400 nT R_M^3 (conversely the Earth's magnetic field moment is 30,000 nT R_E^3) and the dipole axis would be approximately aligned with its spin axis (pointing approximately 10° from the South Pole).

In Table I the main characteristics of the planet are reported and compared to the Earth's values.

1.2. Hermean System: Surface-Exosphere-Magnetosphere

The purpose of the present review is to emphasise how the characterizations of the Hermean exosphere can provide useful information about the magnetosphere, the surface, and the interactions between solar wind and the planet as well as about the evolutionary history of Mercury. We start from the observations of the exospheric compositions to investigate which kind of information we can obtain from them and from new, more accurate, exospheric measurements.

The UV spectroscopic observations on Mariner 10 and ground-based observations of the gaseous envelope of Mercury established the presence of H, He, O,

TABLE I
Mercury's main characteristics[a]

Parameter	Mercury	Earth
Mean orbital axis (AU)	0.387	1
Perihelion (10^6 km)	46	147
Aphelion (10^6 km)	70	152
Eccentricity	0.206	0.017
Inclination to ecliptic	7°	0°
Sidereal orbital period (Earth's day)	87.97	365.26
Sidereal rotation period (h)	1407.6	23.94
Spin axis obliquity to orbit	0.1°	23.4°
Mass (10^{24} kg)	0.33	5.97
Radius (km)	2440	6374
Density (g cm^{-3})	5.43	5.52
Uncompressed density (g cm^{-3})	5.3	4.1
Maximum surface temperature (K)	700	279
Minimum surface temperature (K)	90	
Magnetic field moment	300 nT R_M^3	30000 nT R_E^3
Magnetic axis inclination to spin axis	10°	17°

[a]From the book *Mercury*, Vilas, Chapman and Matthews, (eds.) 1988.

Na, K and Ca (Broadfoot *et al.*, 1976; Potter and Motgen, 1985, 1986; Bida *et al.*, 2000). In Section 2 the observations and estimations of the neutral and ionised components of the exosphere are reviewed.

The column density of the observed constituents is $\leq 10^{12}$ cm^{-2} (Killen and Ip, 1999). Generally, if the total column content of an atmosphere is $N_\infty \leq \sigma^{-1} \cong 10^{14}$ cm^{-2}, where σ is the typical cross section of the gas particles, the gaseous envelope is referred to as "exosphere". Hence, the gaseous envelope of Mercury is uncollisional and with the individual particles travelling along ballistic trajectories. The photo-ionisation of the exospheric atoms creates an ion population (which mixes with the ions directly emitted from the surface), especially in the dayside hemisphere. The Hermean planetary surface, exosphere and magnetosphere, under the influence of the solar wind and interstellar medium, constitute a complex, strongly coupled system, mostly dominated by interactions of the neutral and ionised gas particles with the surface as well as with the magnetospheric plasma. A schematic summary of the interacting processes is shown in Figure 1.

The Hermean exosphere is continuously refilled and eroded by the mentioned interactions. In fact, it would be more correct to consider the Hermean environment as a single system: surface-exosphere-magnetosphere, since these three parts are strongly linked to each other.

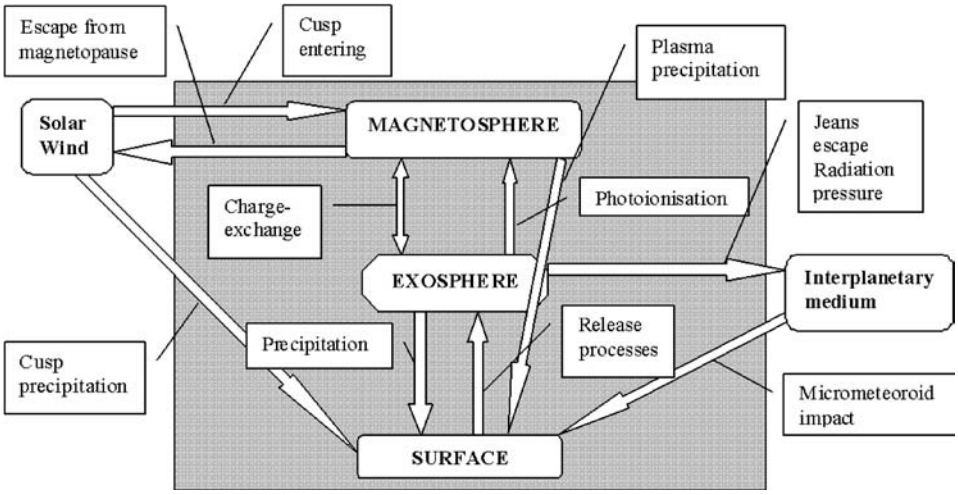

Figure 1. Schematic summary of the interacting processes.

Charge exchange between exospheric neutrals and the solar wind plasma entering through the cusp, is another important process. This process should produce flashes of energetic neutral atoms (ENA) of solar wind origin (Orsini *et al*., 2001; Barabash *et al*., 2001; Mura *et al*., 2004) and thermal ions. These newly born ions together with the ions generated by photo-ionisation from the neutrals and ions produced by the ion-sputtering, quickly energised by the magnetic and electric fields, become part of the Hermean magnetosphere (magnetospheric refilling). Part of the circulating magnetospheric plasma falls back to the planet surface. In any case, since a relevant part of the magnetospheric plasma is lost again in the solar wind (Ip, 1993; Delcourt *et al*., 2003), these interactions are important for the planetary global mass loss. In Section 3 the most suitable models and the most recently developed simulations related to the exosphere-magnetosphere interaction are depicted.

The exosphere is mainly refilled by the surface release processes of neutral or ionised atoms and molecules. The kinetic energy of the released particles depends on the process involved and is below a few eVs for photon-stimulated desorption (PSD) and thermal evaporation, a few eVs for micrometeoroid impact, and can reach higher values for ion sputtering. Even the regions where the exospheric gas is released depend strongly on the active process. Hence, by observing the components of the exosphere, we could gain information on the surface composition and on the release processes acting on the surface (e.g. Killen and Ip, 1999; Wurz and Lammer, 2003). Many of the exospheric atoms and molecules are gravitationally bound, hence they eventually fall back onto the surface; however, Jeans escape is an important loss mechanism for both the lighter and more energetic atoms. Section 4 deals with the exosphere-surface interaction, describing the models of

crust composition and the simulations of the exosphere resulting from the release processes.

In this frame a detailed analysis of

1) Composition and vertical structure (species, spectra and spatial distributions)
2) Dynamics: day to night circulation, active to inactive regions
3) Surface release processes, sources: e.g. regolith, meteorites, etc.
4) Search for ion components and its relation with neutral atmosphere
5) Atmosphere/magnetosphere exchange and transport processes
6) Escape, source/sink balance, geochemical cycles

is crucial for gaining knowledge of the environment and the evolution of Mercury. The next NASA mission (MESSENGER, to be launched in 2004) and the ESA-JAXA (BepiColombo/Mercury Planetary Orbiter, BC/MPO, and Mercury Magnetospheric Orbiter, BC/MMO, launch scheduled for 2012 (Balogh *et al*., 2000)) joint mission will hopefully address a lot of these issues, thanks to the instrumentation planned for the payloads'. In Section 5 we give some additional information about the potential of future measurements, with particular emphasis on the potential of *in situ* detection of ions and neutral atoms for exosphere investigation.

2. The Exosphere

2.1. Exosphere Observations: Extension and Composition

Mercury, because of its proximity to the Sun and its small size, has not been able to retain its atmosphere. However, the existence of gaseous species H, He and O has been observed by the UVS-instrument on Mariner 10 (Broadfoot *et al*., 1976). Since the Mariner 10 fly-bys, the exosphere of Mercury has been observed in the Na (Potter and Morgan, 1985, 1990) and K (Potter and Morgan, 1986) D lines. Calcium has been observed in the polar exosphere (Bida *et al*., 2000). Radar-bright regions have been discovered at the poles, attributed to volatile deposits (water or sulphur) in permanently shadowed craters (Harmon and Slade, 1992; Ingersoll *et al*., 1992; Paige *et al*., 1992; Butler and Muhleman, 1993; Butler, 1997; Sprague *et al*., 1995, 1996a; Harmon *et al*., 1994; 2001; Starukhina, 2000).

As will be emphasised in Section 5, many instruments on board the two upcoming missions will use remote sensing as well as *in situ* measurements to determine the exact exospheric composition and element distribution. In fact, it is expected that the six observed elements constitute only a small fraction of Mercury's exosphere, because at the surface the total pressure, derived from the sum of these known species, is almost two orders of magnitude less than the exospheric pressure of approximately 10^{-10} mbar, obtained by the Mariner 10 occultation experiment (Fjelbo *et al*., 1976; Hunten *et al*., 1988). In Table II the atmospheric abundances and loss rates as estimated and/or measured are reported. Note that some of the

TABLE II
Atmospheric abundances and loss rates

Species	Surface abundance (cm^{-3})	Total Zenith column (cm^{-2})	Jeans flux (cm^{-2} s^{-1}) $T = 550$	Photo-ionisation lifetime (sec) $R = 0.386$ AU	Photo-ionisation rate (cm^{-2} s^{-1}) $R = 0.386$ AU
H	23; 230[a]	3×10^{9}[h]	2.7[l]	2.0×10^{6}[l]	1.5×10^{3}[l]
He	6.0×10^{3}[a]	$<3 \times 10^{11}$[h]	5.3[l]	2.83×10^{6}[l]	1.1×10^{5}[l]
Li		$<8.4 \times 10^{7}$[n]			
O	$4.4 \times 1\,0^{4}$[a]	$<3 \times 10^{11}$[h]	6.3×10^{-9}[l]	7.43×10^{5}[l]	4.0×10^{5}[l]
^{20}Ne	6×10^{3} day[c]				
	7×10^{5} night[c]				
Na	1.7–3.8 $\times 10^{4}$[a]	2×10^{11}[i]	6.9×10^{-15}[l]	5500–14000[m−]	2.1×10^{7}[m−(e)]
				14000–38000[m−]	7.4×10^{6}[m−(t)]
				25000[q]	
Mg	7.5×10^{3}[d]	3.9×10^{10}[d]			
Al	654[c]	3.0×10^{9}[d]			
Si	2.7×10^{3}[d]	1.2×10^{10}[d]			
S	5×10^{3}[d]	2.0×10^{10}[d]		1.3×10^{5}[l]	1.5×10^{5}[l]
	6×10^{5}[g]	2.0×10^{13}[g]			1.5×10^{8}[l]
Ar	$<6.6 \times 10^{6}$[a]	$<9 \times 10^{14}$[h]		4.8×10^{5}[l]	4.2×10^{7}[l]
		1.3×10^{9}[k]			
K	3.3×10^{2}[b]	2×10^{9}[b]		6700[m]	1.5×10^{5}[l]
	5×10^{2}[h]				
Ca	387[d]	$<1.2 \times 10^{9}$[d]			
	<239[f]	$<7.4 \times 10^{8}$[e]			
		1.1×10^{8}[j]			
Fe	340[d]	7.5×10^{8}[d]			
H_2	$<1.4 \times 10^{7}$[p]	$<2.9 \times 10^{15}$[p]		2.3×10^{6}[l]	8.8×10^{8}[l]
O_2	$<2.5 \times 10^{7}$[p]	$<9 \times 10^{14}$[p]		2.6×10^{5}[l]	2.7×10^{9}[l]
N_2	$<2.3 \times 10^{7}$[p]	$<9 \times 10^{14}$[p]		4.1×10^{5}[l]	4.5×10^{4}[l]
OH	1.4×10^{3}[d,e]	1×10^{10}[d,e]		6.2×10^{5}[l]	2.7×10^{6}[l]
CO_2	$<1.6 \times 10^{7}$[p]	$<4 \times 10^{14}$[p]		1.9×10^{5}[l]	2.0×10^{8}[l]
H_2O	$<1.5 \times 10^{7}$[p]	$<1 \times 10^{12}$[e]		3.7×10^{5}[l]	2.0×10^{8}[l]
		$<8 \times 10^{14}$[p]			

[a]Hunten *et al*. (1988): measurements or upper limits; [b]Potter and Morgan (1997a); [c]Hodges (1974): model abundance; [d]Morgan and Killen (1997): model abundances; [e]Killen *et al*. (1997a): model abundances; [f]Sprague *et al*. (1993): measured upper limit; [g]Sprague *et al*. (1995, 1996a): prediction; [h]Shemansky (1988): Mariner 10 measurements; [i]Killen *et al*. (1990): measured abundance; [j]Bida *et al*. (2000); [k]Killen (2002a): model abundance; [l]Killen and Ip (1999); [m]Huebner *et al*. (1992) ionisation rates: experimental (e) theoretical (t) for quiet and active Sun; [n]Sprague *et al*. (1996b): model abundance; [p]Broadfoot *et al*. (1976); [q]Cremonese *et al*. (1997).

reported species (such as N_2, O_2, CO_2 and H_2O) are just estimated as upper limits and their existence in the Hermean exosphere has to be confirmed by observations. The Jeans flux is estimated only for lighter atoms since Jeans escape is negligible for heavier atoms.

2.1.1. *Hydrogen and Helium*

The H and He distributions were measured above the subsolar point from the UVS 1216 Å and 584 Å channels, respectively, onboard Mariner 10 (Broadfoot *et al.*, 1976). The scale height of He above the subsolar point corresponds to a temperature of 575 K with surface number densities of 6,000 cm^{-3}. The distribution of H above the subsolar point revealed two thermal components characteristic of a dayside temperature (420 K) and a nightside temperature (110 K) with surface number densities of 23 and 230 cm^{-3}, respectively (revised by Shemansky, 1988). Explanations for the cold component at the subsolar point include a nightside source (Shemansky and Broadfoot, 1977), photolysis of water (Broadfoot *et al.*, 1976), or surface chemistry (Potter, 1995). In any case, the presence of so much cold H on the dayside is surprising and not yet understood. No day/night asymmetry in the H abundance is expected, because of the mobility of H and the lack of energy accommodation. However, the distribution has only been measured normal to the limb at the subsolar point.

2.1.2. *Oxygen*

The oxygen reservoir in the atmosphere is probably comparable to that of Na or slightly larger (Shemansky, 1988). The small amount of observed atmospheric oxygen relative ($<4.10^4$ cm^{-3}) relative to the surface stoichiometry ($\approx$50%) may indicate that atmospheric oxygen is bound in molecules, or it may indicate inefficient release (Morgan and Killen, 1997), or it may efficiently charge exchange with solar wind and magnetospheric protons. It has been suggested that the lunar oxygen can be driven out from the atmosphere by photo-ionisation and subsequently carried away in the solar wind (Morgan and Shemansky, 1991), and the Hermean conditions could be quite similar. Among the known atmospheric constituents only O is expected to have a substantial nightside enhancement, about 100 times more than that of the dayside, since this species requires more time to thermalise (has a high thermal accommodation time) (Hodges and Johnson, 1968; Hunten *et al.*, 1988); nevertheless, we have no observations to confirm this expectation.

Furthermore, at Mercury it is expected that the isotopic composition of oxygen (^{16}O, ^{17}O, ^{18}O) is different from other solar system objects (Terrestrial ratios are $^{18}O/^{16}O = 1/490$, $^{17}O/^{16}O = 1/2700$, e.g. Clayton, 2003) because: a) the past mass-dependent escape of gases from the planetary environments; b) the preservation of interstellar materials within the planet; c) the processes involved in the formation of the solar nebula, protoplanetary disks and planets. Even if determining the isotopic ratio is not an easy task, particularly intense events of ion-sputtering (during active periods) and additional Oxygen atoms produced by dissociation of

exospheric Oxygen compounds could lead to a strong oxygen signal, up to 10^5 cm^{-3} (see Section 4), useful for a determination of the $^{18}O/^{16}O$ ratio, at least. This estimation could provide crucial insight into the planet's evolution (e.g. Lammer *et al*., 2000).

2.1.3. *Sodium and Potassium*

Although the surface abundance of Na and K is in the *per mille* range (Wurz and Lammer, 2003), and although their relative ratio is of the order of 100 (Potter *et al*., 2002b), we have several observations by ground-based telescopes because of their strong resonance lines. Potter and Morgan (1985) estimated a total column abundance of Na based on the D2/D1 ratio (N) of 8.1×10^{11} atoms cm^{-2}, which later was corrected to $1 - 3 \times 10^{11}$ cm^{-2} by Killen *et al*. (1990). The most fascinating feature of the Na and K distributions is the presence of high latitude enhancements, which appear and disappear on timescales less than one day (see Figure 2). The early observations showed that the distribution of the alkalis is often peaked in the high to mid-latitudes, whereas it decreases toward the terminator and is highly time variable (Potter and Morgan, 1990; Killen *et al*., 1990). The high-latitude enhancements were confirmed via observations of Na with an echelle spectrograph and an image slicer, providing full coverage of the Mercury exosphere at one time (Potter and Morgan, 1990; 1997a; Potter *et al*., 1999) and it can be seen as evidence of magnetospheric processes (Potter and Morgan, 1990), or local surface concentration enhancements due to sodium migration from the dayside to the nightside and subsequent reimplantation on the nightside preferentially in high-latitude regions (Leblanc and Johnson, 2003), or perhaps associated with the radar bright terrains (Sprague *et al*., 1997). An ion sputter source (Killen *et al*., 1990; Potter and Morgan, 1990) would be expected to vary sporadically, and to show correlations with the solar cycle. The observations of Na abundance appear to be consistent with a mixture of sources: ion sputtering at high latitudes and photon-stimulated sources, meteoritic vapourisation and/or chemical sources at low latitudes. Killen *et al*. (1990) reported that the sodium is displaced sunward except for the high radiation pressure case.

Dawn/dusk asymmetries in Na and K have been reported and summarised by Sprague *et al*. (1997). These asymmetries were attributed to ion implantation in the uppermost 50 Å surface layer during Hermean night with subsequent degassing on the morning terminator (Sprague, 1992; Leblanc and Johnson, 2003). Killen and Morgan (1993) also argued that a body of observations exists which shows no sunrise/sunset column differences.

Although the Na exosphere was initially reported to be thermally accommodated with the surface at about 550 K (Potter and Morgan, 1987), more recent observations indicate that a substantial, perhaps dominant, suprathermal component exists (Potter and Morgan, 1997b). Recent evidence indicates that the source atoms are hot (Killen *et al*., 1997b, 1999; Potter and Morgan, 1997b; Bida *et al*., 2000), favouring a more energetic process for their release than thermal evaporation. For instance, the line

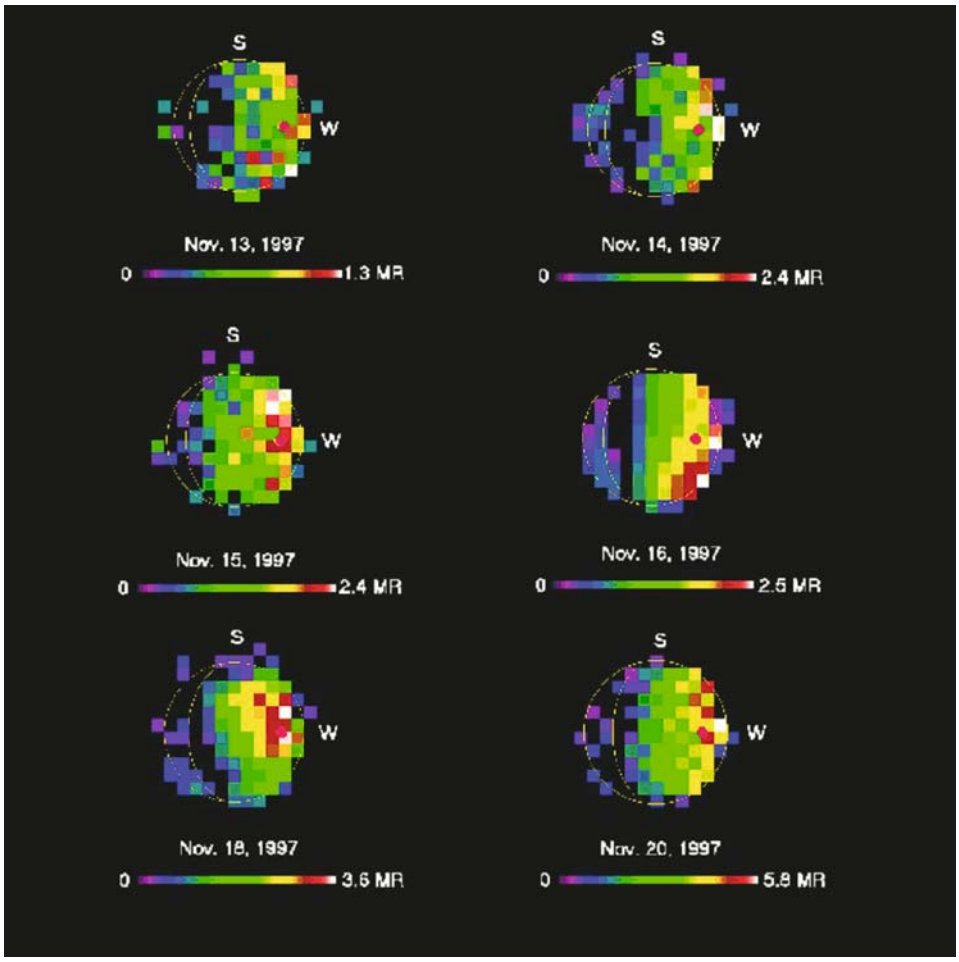

Figure 2. Images of Mercury's Na D_2 emission in MegaRayleighs observed on November 13–20. The subsolar point is marked with a red dot (Potter *et al.*, 1999). It should be noted that the high latitude enhancements have strong variation in intensity and profile, on timescales less than one day.

profiles (show that the temperature of the sodium is about 750 K at the poles and 1,200 K at the equator (Killen *et al.*, 1999). It came as a surprise when a very hot Na corona was imaged by Potter and Morgan on October 24, 1995, using an image slicer at the McMath-Pierce solar telescope (Potter and Morgan, 1997b). A substantial sodium tail, predicted by Ip (1986), has recently been imaged (see Figure 3), where sodium emission is seen up to thousands of kilometres above the planetary surface in the anti-sunward direction. The atoms observed in Mercury's sodium tail represent those atoms initially in the high-velocity tail of the source distribution that have initial velocities greater than 2.1 km/sec (Smyth, 1986). These atoms represent about 10% of the source population (Potter *et al.*, 2002a). Observations are needed in order to confirm such a hypothesis. However, recently Leblanc and Johnson

(2003) reproduced the column density and velocity profiles along Mercury's sodium tail as measured by Potter *et al*. (2002a) with a good agreement and concluded, in agreement with them, that the characteristics of these profiles are mainly induced by solar radiation pressure acceleration of the sodium atoms and cannot be related to their processes of ejection at Mercury's surface. Actually, in Leblanc and Johnson (2003) more than 85% of the sodium atoms in Mercury's exosphere are released by thermal desorption.

Potassium was discovered in the Hermean exosphere a year after the Na discovery was reported (Potter and Morgan, 1986). The average column abundance is 10^9 atoms cm^{-2}, with large variations. There are fewer observations of K than of Na. Even though the scattering efficiency of K is greater than that of Na (Shemansky, 1988), its abundance is about two orders of magnitude less than that of Na, and the K D2 line is often obscured by telluric O_2 absorption. There is one published image of the K exosphere (Figure 4), showing that the morphology is roughly similar to that of Na. Sprague *et al*. (1990) reported a significant enhancement (by a factor of 3.6) of potassium seen when Caloris basin was in view (1987 October 14). The observation was attributed to increased diffusion in the Caloris basin region from a deep source; but this interpretation was challenged by Potter and Morgan (1997a) and by Killen *et al*. (2001) who suggested that any enhancement over Caloris is consistent with time-variability seen in other longitude ranges not associated with any geological features.

2.1.4. *Calcium*

The neutral calcium abundance reported by Bida *et al*. (2000) is consistent with the predicted planetary average column abundance for Ca for a 'volatile' composition, 6.4×10^8 cm^{-2} (Morgan and Killen, 1997), but the observations can be related to ion-sputtering or to impact vapourisation processes. Morgan and Killen (1997) argued that Ca atoms should be released less efficiently than Na because its binding energy with O (4.8 eV) is almost twice that of the Na–O bond (2.6 eV). However, it is likely that Ca is released in the molecular form, possibly as CaO. If so, CaO could be dissociated in the atmosphere, for instance by Lyman α photons, giving the Ca atom excess energy as observed (Killen *et al*., 2004b). In addition, because Ca is refractory, it is likely to be adsorbed at the surface upon contact, whereas Na will be efficiently released at the surface temperatures on the dayside. The lifetime of an Na atom in the exosphere is affected by photo-ionisation (between 5,000 and 20,000 s, see Table II), whereas the lifetime of Ca is probably the ballistic lifetime (about 950 s). The available data do not rule out a more intermediate crust composition. A time series of spatially resolved observations would enable us to separate the effects of source processes, which are likely to be spatially and temporally variable, and crust composition, which may be spatially inhomogeneous but shouldn't vary on short time scales. Since Ca is refractory it may be considered as a tracer of ion sputtering. In fact, less energetic processes (e.g. PSD see Section 4)

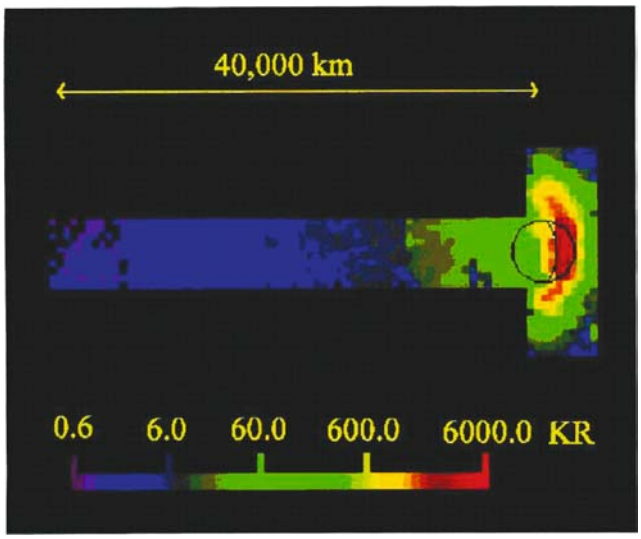

Figure 3. Images of the sodium D_2 emission intensity in kiloRayleighs downstream (anti-sunward) of Mercury at 0300 UT May 26, 2001. Each square represents an observation with the 10×10 arcsec image slicer, and represents an area 5100 km on a side. These observations are tailored towards measurement of the downstream profile of the tail along its axis. West is on the right and South is at the top of the figure. (Potter *et al.*, 2002a).

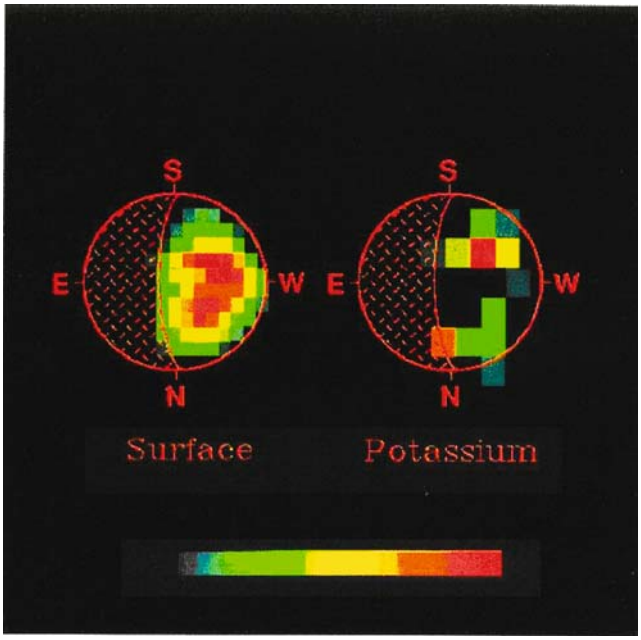

Figure 4. Images of Mercury in 7670–7680 Å sunlight reflected from the surface and in sunlight scattered at 7664 Å from potassium vapour in the Mercury atmosphere. The measurements were made on December 7, 1990 (Potter and Morgan, 1997a).

are not efficient in ejecting the Ca atoms as well as the other refractory elements from the mineral surface.

2.1.5. *Argon*

The diurnal variation of the surface abundance of Ar seen in the lunar atmosphere is also expected at Mercury. Ar was seen to condense on the lunar nightside and to evaporate at dawn. Because it flows from dawn to the nightside, the argon abundance rises in the pre-dawn sector. Differences in the diurnal behaviour of the Ar and Na gases are significant because the Na residence time in the exosphere is shorter (1.5 h at perihelion) than that of Ar (perhaps 36 h). McGrath *et al*. (1986) and Killen *et al*. (2001) argued that the alkalis are probably preferentially derived from the surface by PSD which increases as the inverse square distance from the Sun. In contrast, argon, being a noble gas, easily diffuses through a rock (e.g. Mussett, 1969), and readily escapes from the surface into the exosphere (Hodges, 1975; Hodges *et al*., 1973). Since Argon at thermal energies is confined near the surface, the probability that Ar^+, if ionised in appreciable amounts, is recycled to the surface is far greater than that probability for Na ions. Hence, the Ar reservoir may be longer lived than the Na reservoir. Killen (2002a) predicts global average column abundance at Mercury similar to that at the moon, corresponding to 1.3×10^9 atoms cm^{-2}, four orders of magnitude less than the upper limit ($<10^{13}$ atoms cm^{-2}) given by the Mariner 10 results.

2.2. Ions of Planetary Origin

Ions of planetary origin in the Hermean environment have not yet been observed, nevertheless, as stated before, the photo-ionisation of the exospheric atoms creates ionised thermal populations, especially in the dayside. A second source of planetary ions is established via particle sputtering since the impact of energetic ions (of solar wind or magnetospheric origin, see Section 3) not only causes the release of neutral particles but also direct release of ions from the planetary surface. The fraction of released ions is about 1% of the released neutrals. Sputtered ions have characteristic energies of a few eV, similar to sputtered atoms (Section 4).

The ion populations, originating mainly from these two mechanisms, can hardly be considered as an ionosphere, able to shield the magnetic and electric fields of the magnetosphere; hence, in the following we refer to it as exo-ionosphere. In this frame, the ions are energised immediately and become part of the magnetospheric ion populations, together with the solar wind plasma entering through the cusp regions. The magnetospheric plasma partially impacts on the surface (Ip, 1997; Delcourt *et al*., 2003); the plasma particles are absorbed by the surface at specific latitudes (Delcourt *et al*., 2003; Leblanc *et al*., 2003) and are redistributed over the planetary surface (Killen *et al*., 2004a). On the other hand, part of the magnetospheric plasma is eventually lost to the solar wind (Ip, 1997; Delcourt *et al*., 2003) (see Section 3). Ion measurements are important for the planet's global mass

loss estimation and provide key information about the formation and the erosion of Mercury's neutral exosphere.

The photo-ionisation lifetimes are given in Table II and these times have to be compared with ballistic travel times of the order of 1000 s. One realises that for some species, such as Li, Na, Mg and K, the photo-ionisation lifetimes are sufficiently small that there is a reasonable probability of these species becoming ionised during their trajectory in the exosphere. Lundin *et al*. (1997) estimated the ion density from neutral density as being equal to $n_i = n_n T_c/\tau_{ph}(1/\beta)$ where n_n is the neutral density of the considered species, T_c its gyroperiod and β the escape fraction (maximum ion density is obtained for $\beta = 1$), τ_{ph} is the photo-ionisation life-time. They estimated 10^{-3} He^+, 0.1 O^+, 10 Na^+ and 0.5 K^+ ion density (cm^{-3}) at the surface at the subsolar point.

Recently, Leblanc *et al*. (2004) considered all the uncertainties that possibly could arise from:

- the surface binding energy, which affects the energy and the efficiency with which a particle is ejected from the surface by ion or photon sputtering (see Section 4). This is important for most refractory elements (Fe, Ni, Si, Al, Mg, Cl, Kr, Xe and Ca) which are essentially ejected by ion sputtering.
- the regolith composition. Goettel (1988) suggested several possible compositions of Mercury's regolith with variations of abundances for Al, Ca, Fe, Na and Ti by up to a factor of 5. For volatiles the depletion of the surface induced essentially by thermal desorption could also have an important impact on the local exospheric density.
- the porosity of the surface material could reduce by up to a factor of 5 (Hapke, 1986; Johnson, 1989) the efficiency of the processes of ejection from the surface as estimated from theoretical works or laboratory experiments.
- the efficiency by which a species is lost from Mercury's exosphere, i.e. direct neutral loss, ionization and further loss induced by the solar wind electric field of convection or reabsorption at the surface. In the same way, the source of fresh material for Mercury's exosphere, which can be due to regolith diffusion, meteoritic gardening and deposition, solar wind implantation or ion planetary reimplantation, could change any estimate of the surface composition.
- the main process by which a species is ejected from the surface. As an example, ejection of O atoms from the surface via either particle sputtering or impact vapourisation will produce a density profile less sharp, hence one may overestimate the capability of O atoms to reach high altitudes. In the case of low energetic surface release processes like photon stimulated or thermal desorption only a fraction of the heavy elements (Lammer *et al*., 2003) will reach high altitudes as neutrals.

At the end, Mercury's exosphere is far from being spherically homogeneous, which implies, in particular, a wide range of possible variations of the density of both neutral and ion species. Leblanc *et al*. (2003) have shown that the Na^+ density

could spatially vary between 10^{-2} and 10 Na^+/cm^3 at Mercury's surface, whereas the Na neutral distribution is more uniform around Mercury at an altitude of about 400 km. Generally, at this altitude the expected ion densities (for instance of H^+, He^+, O^+, Na^+, Si^+, S^+ and Mg^+) range between 10^{-4} and 10^2 (Leblanc *et al.*, 2004).

The day/night and perihelion/aphelion asymmetries in the ion production strongly depend on the adopted exosphere model. In the Wurz and Lammer (2003) exospheric simulation the densities maximise near the planetary surface in the dayside sector at the perihelion since the solar wind and photon flux are maximal there. Nevertheless, dynamical coupling of the planetary motion, the release processes and the ion circulation could lead to a denser Na^+ "exo-ionosphere" at the aphelion than at the perihelion in relation with the denser Na exosphere at the aphelion than at the perihelion predicted by Leblanc and Johnson (2003) (see Section 4).

As will be better described in Section 5, the ion spectrometers of the BepiColombo mission will be able to determine the ion composition and energy in the Hermean environment.

3. Exosphere-Magnetosphere Interaction

3.1. Solar Wind and Interplanetary Magnetic Field at 0.3 AU

The solar wind at Mercury's orbit (0.30–0.47 AU, mean distance = 0.387 AU) differs substantially from the average conditions present at 1 AU. The Parker spiral forms an angle of about 20° with the solar wind radial direction, less than half of the value at Earth's orbit (∼45°); this implies a change of the relative ratio of the Interplanetary Magnetic Field (IMF) components with respect to the near Earth conditions, thus modifying the solar wind-magnetosphere relationship. Therefore, the contribution of the IMF B_y component (in the planetary Solar Magnetic coordinates) is less relevant than at the Earth, so that the magnetic reconnection at the dayside magnetopause is essentially driven by the IMF B_z component. Moreover, the increasing weight of the IMF B_x component might play a role in the way that Mercury's magnetosphere links with the solar wind (e.g. Killen *et al.*, 2001; Kallio and Janhunen, 2003a). The average solar wind density is about ten times higher than that at Earth, but this value varies considerably due to the high eccentricity of the orbit of the planet: in fact, using the formula derived from the data of Helios spacecraft between 0.3 and 1.0 AU (Bougeret *et al.*, 1984):

$$N = 6.4 \times R^{-2.1}\ \mathrm{cm}^{-3} \tag{1}$$

where $N_{\min}$ is the 32 cm^{-3} at the aphelion (0.47 AU), $N_{\max}$ the 73 cm^{-3} at the perihelion (0.31 AU) and N_{ave} the 46 cm^{-3} (0.39 AU), compared to $N \sim 6\ cm^{-3}$ at 1 AU. Table III reports some important average values, referred to slow solar wind,

TABLE III
Solar wind parameters at Mercury

Parameter	Average	Perihelion	Aphelion
Solar wind speed (km/s)	430	430	430
Solar wind density (cm^{-3})	46	73	32
Dynamic pressure (nPa)		16	
IMF (nT)	30	46	21
Spiral angle (deg.)	21°	17°	25°
Proton temperature (K)	15×10^4	17×10^4	13×10^4
Electron temperature (K)	20×10^4	22×10^4	19×10^4
Ion sound speed (km/s)		74	70
Alfvén speed (km/s)	97	120	82
Specific heat ratio (γ)	5/3	5/3	5/3
Mach number (M_∞)		5.8	6.1
Alfvénic Mach number ($M_{A\infty}$)	4.4	3.6	5.2

evaluated at 0.39 AU (data from Kabin *et al*., 2000) and at perihelion and aphelion (Slavin and Holzer, 1981; Russell *et al*., 1988).

3.2. The Hermean Magnetic Field and Solar Wind Interaction, Comparison with Terrestrial Conditions

Magnetic measurements during the first and third Mariner 10 fly-bys in March 1974 and March 1975 clearly provided evidence of an intrinsic magnetic field (see Figure 5) the estimated dipole moment ranges between 284 and 358 nT R_M^3, with the same polarity as the present dipole moment of the Earth's and more or less aligned with the rotation axis of the planet (see Table I). During the Mariner 10 fly-bys, measurements of energetic electrons (Ogilvie *et al*., 1977) provided information on the bow shock and magnetopause distance.

Even though the origin of the internal field is still uncertain (e.g. Schubert *et al*., 1988), it seems that the Hermean magnetosphere is in many respects a miniature of the Earth's magnetosphere. The size of the Hermean magnetosphere is only 5% of that of the Earth, although the planetary radii differ by less than a factor of 3. The subsolar distance of the magnetopause is $\cong 10\ R_E$ at the Earth, while it is $\cong 1.6\ R_M$ at Mercury (Siscoe and Cristofer, 1975; Goldstein *et al*., 1981), hence, in a zero order analysis, the spatial dimensions must be scaled by a factor of ~ 7 or 8 (Ogilvie *et al*., 1977; Russel *et al*., 1988). Therefore, the planetary body occupies a much larger fraction of the magnetosphere than in the Earth case (see Figure 6).

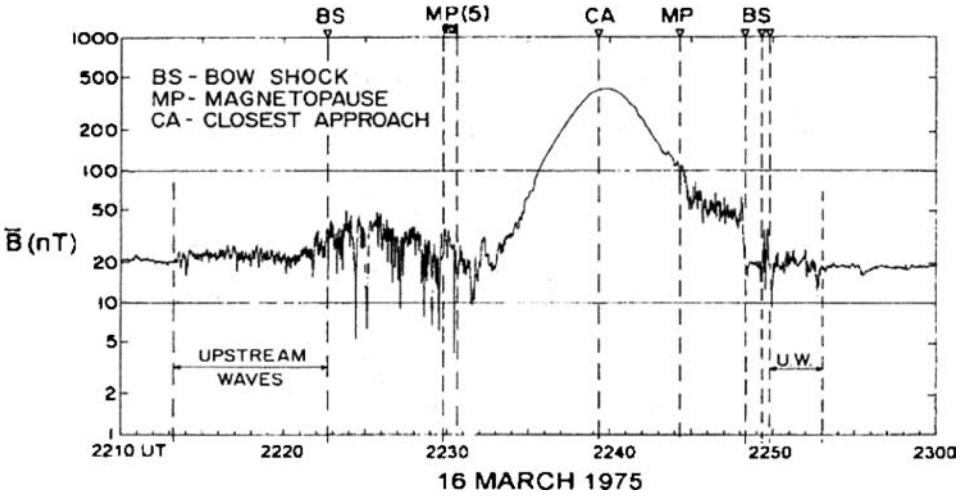

Figure 5. Magnetic field observations during Mariner 10, third encounter with Mercury (Ness *et al.*, 1975).

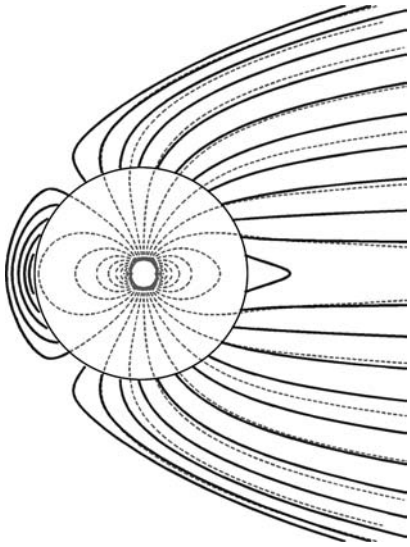

Figure 6. Schematic comparison between the Earth's (red) and Mercury's (black) magnetosphere scaled to the subsolar distance of the magnetopause.

The time scale variations of the magnetospheric processes are tens times shorter at Mercury compared with Earth (a few minutes compared to $\cong$1 h at the Earth) (Siscoe *et al.*, 1975).

Due to the small temporal and spatial scale, it is likely that the solar wind parameters are more significant for the characteristic features of the planet's magnetosheath and magnetosphere, especially considering the connection of the Hermean magnetosphere to the IMF (Luhmann *et al.*, 1998). In particular, the possible role

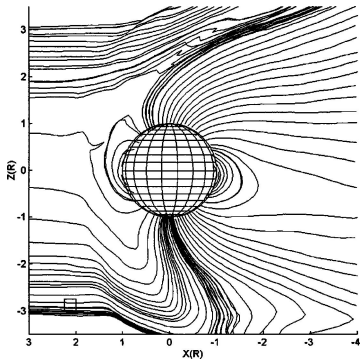

Figure 7. Morphology of the magnetic field near Mercury in the Parker spiral angle type of IMF case (IMF = (32, 10, 0) nT). The lines show the magnetic field lines derived from a self-consistent kinetic model (Kallio and Janhunen, 2004).

of the IMF has been a subject of Hermean magnetosphere studies based on both analytical (Sarantos *et al*., 2001) and self-consistent numerical studies (Gombosi, 2000; Kabin *et al*., 2000; Ip and Kopp, 2002; Kallio and Janhunen, 2004). The self-consistent simulations have evidenced that, when the IMF x-component is strong, the magnetic field morphology and the magnetic reconnection are quite different from the Earth's case, thus giving different plasma entry and circulation in the magnetosphere (see Figure 7).

It has been speculated that, occasionally, the pressure of the solar wind may be large enough to push the magnetopause against the surface of the planet (Goldstein *et al*., 1981), for example, during strong coronal mass ejections. Both MHD (Kabin *et al*., 2000) and quasi-neutral hybrid models (Kallio and Janhunen, 2004) support such an hypothesis.

3.3. Energetic Particles in Mercury's Environment

From the Mariner 10 measurements (Figure 8), Slavin *et al*. (1997) inferred a field-aligned current of the order of 10^6 A, comparable to the typical values at Earth. The dynamic variation observed has many characteristics in common with substorm activity (e.g. Siscoe *et al*., 1975; Eraker and Simpson, 1986; Slavin *et al*., 1997; Ip, 1997). Nevertheless, the Earth's ionosphere allows the closure of the magnetospheric currents, while Mercury does not have an ionosphere, but may have only an exo-ionosphere (see Section 2.2). The observed currents would then require a sufficiently conducting layer close to or on Mercury's surface (Kabin *et al*., 2000). Cheng *et al*. (1987) suggested that Na^+ or other heavy ions could be picked up by the solar wind and energised, thus producing a Pedersen conductance of the Hermean exosphere. Janhunen and Kallio (2004), recently, studied how the surface conductivity acts in modifying the magnetosphere configuration. They found that

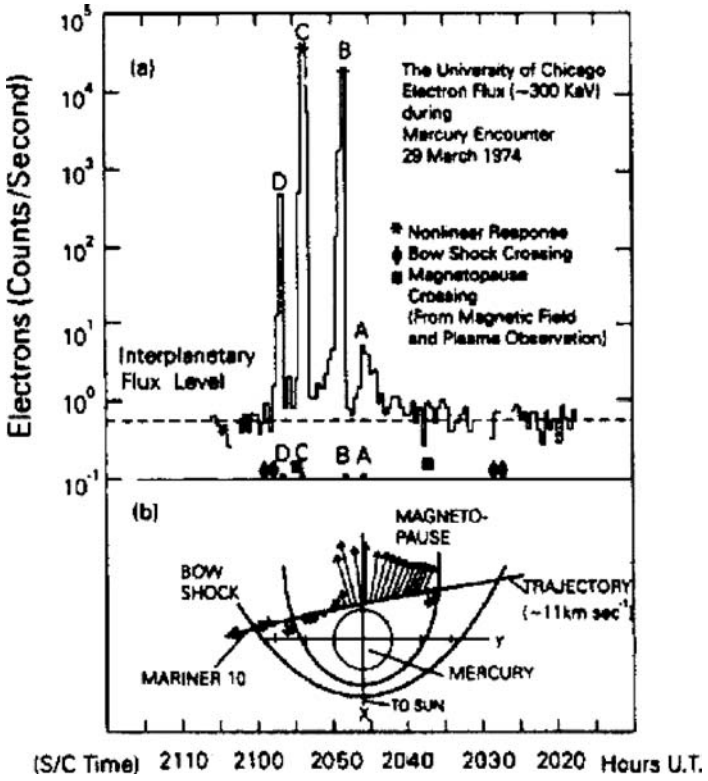

Figure 8. Measurements of energetic electrons and protons (a) and magnetic field variations (b) during the first Mercury passage of Mariner 10 on March 29, 1974 (Simpson *et al*., 1974; Ness *et al.*, 1975).

horizontal differences in the surface conductivity may be the sources of global asymmetry in the magnetosphere. However, the way in which the field-aligned currents close is still debated.

3.3.1. *Magnetospheric Plasma Sources*

The Hermean magnetosphere is populated by ions of essentially two main origins: the solar wind plasma and the ions of planetary origin as discussed above. Both these ion sources are basically located on the dayside, where the solar wind plasma can enter the magnetosphere thanks to the magnetic reconnection of the IMF with the planetary magnetic field (cusp region), and where the exospheric ions are generated by the solar photons interaction with the neutral exosphere as discussed above. In the complex Hermean system, nevertheless, ions could be generated by photo-ionisation or electron impact not only on the dayside, but also in the extended exosphere, and the solar wind could enter through the magnetic tail region.

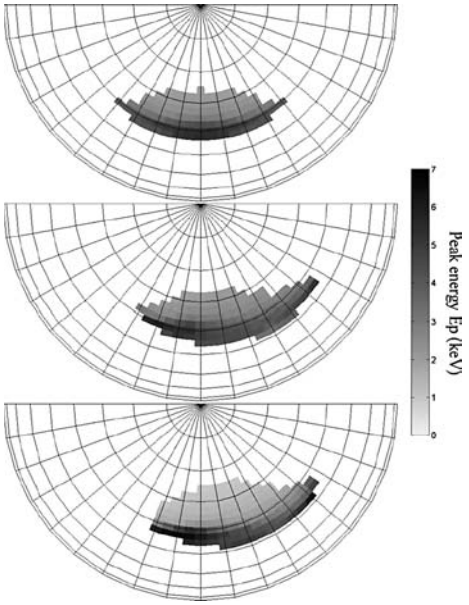

Figure 9. Position and extension of the open field lines area, mapped on the northern dayside surface of Mercury, in response to different solar wind conditions. The area is gray-coded according to the peak energy of the particle distribution. Only the open field lines that cross the magnetopause within 2 R_M are mapped (the field lines at higher latitudes are open indeed, but the rate of solar wind plasma entry is low, since they map far in the magnetic tail), by using a 5° long, per 2.5° lat. grid. The three configurations were calculated for: $P_{dyn} = 16$ nPa, $B_y = 0$ nT and $B_z = -10$ nT (top panel), $P_{dyn} = 16$ nPa, $B_y = -5$ nT and $B_z = -10$ nT (middle panel), $P_{dyn} = 60$ nPa, $B_y = -5$ nT and $B_z = -10$ nT (bottom panel) (Massetti *et al.*, 2003).

3.3.1.1. Solar Wind Source. When the IMF has an anti-parallel component to the magnetospheric field near the magnetopause, i.e. the high-latitude field lines connect to the interplanetary field during southward or sun-ward pointing IMF (Luhmann *et al.*, 1998; Sarantos *et al.*, 2001), a magnetic reconnection occurs between the two fields, and the magnetosheath plasma can cross the magnetopause and precipitate toward the planet, eventually permitting the solar wind plasma entry through open field lines on the dayside surface of Mercury (e.g. Killen *et al.*, 2001; Massetti *et al.*, 2003). The three panels of Figure 9 show position, extension of the open field lines area, and energy distribution mapped on the northern dayside surface of Mercury in response to different solar wind conditions.

Massetti *et al.* (2003) noticed that most of the energy (and flux estimated around 10^9 cm^{-2} s^{-1}) of the precipitating magnetosheath particles is deposited on a region that is narrow in latitude, but conversely extended in longitude. This region can be identified, by analogy with the Earth's magnetosphere, as part of the open low-latitude boundary layer that is linked to the IMF, while the remaining area is characterised by a monotonic decrease of both energy and flux of the precipitating

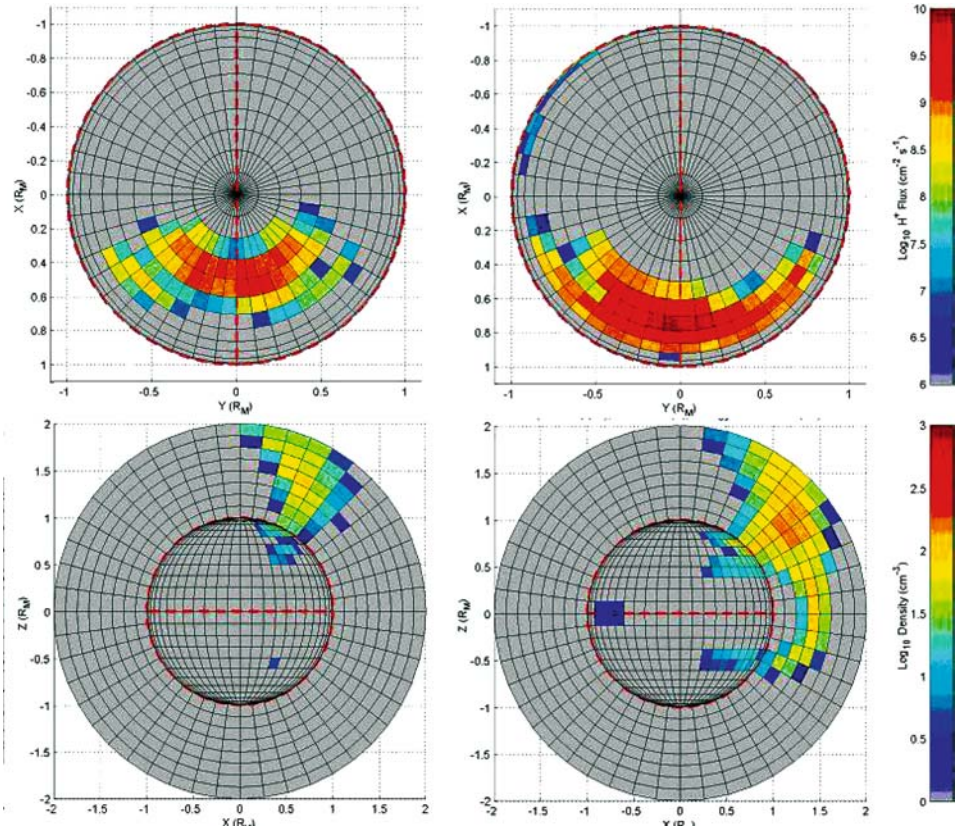

Figure 10. (Panels A and B) Colour-coded maps of H^+ flux over Mercury's surface, as obtained by the three-dimensional trajectory computations by Mura *et al*. (2004); Panel A refers to protons with energies between 0.1 and 1 keV; Panel B refers to energies between 1 and 10 keV. (Panels C and D) Density over two different surfaces: x–z plane (outside the red circle) and Mercury's surface (inside); Panel C refers to protons with energies between 0.1 and 1 keV; Panel D refers to energies between 1 and 10 keV. The boundary conditions are: B = (0, 0, −20) nT and Potential Drop = 10 kV.

particles. A typical open field area of Mercury's cusps during moderate southward pointing IMF, under the assumption of a typical solar wind pressure at 0.39 AU (16 nPa) ranges between about 45° and 65° in latitude, and about −40° and 40° in longitude. Different IMF orientations and solar wind conditions cause the open area to shift in latitude and longitude, and to vary its extension. Recently three-dimensional trajectory computations by Mura *et al*. (2004) of the solar wind protons penetrating the magnetosphere through the cusps show that the precipitating area is not exactly the open field lines projection onto the planetary surface. In fact, the lower energy (<1 keV) protons are more sensitive to the $\mathbf{E} \times \mathbf{B}$ drift (north oriented); hence, they drift northward (Figure 10, Panel C) and impact close to the polar regions (Figure 10, Panel A); the magnetic field drift produces higher-energy (>1 keV) ions precipitating dawn-ward (Figure 10, Panel B).

It can be assumed, approximately, that about 50% of the magnetosheath plasma on reconnected field lines actually crosses the magnetopause (the remaining 50% is reflected by the boundary) (Massetti *et al*., 2003, and references therein). The ions entering the magnetosphere:

– partially (all the planet-directed particles with a pitch angle smaller than 35°) reach the planet surface causing ion sputtering, hence producing neutral atoms with energies up to hundreds of eV (see Section 4);
– are diffused toward closed field lines (since the gyro-radius is not small compared to the open field line area) and circulate in the magnetosphere (see next subsection);
– partially exchange their charge with the thermal exospheric atoms (see Section 3.4), hence producing a Hydrogen-ENA signal in the keV range.

3.3.1.2. Exospheric Ions Source. The ions of planetary origin at Mercury are constituted by the photo-ionised exosphere atoms (as described in Section 2.3) and by the ion component of ion-sputtering process (see Section 4.3). Such ions, confined by the magnetic field, start to circulate within the magnetosphere (see next subsection).

The density, location, species and initial energy of the planetary ions depend both on the process involved in the generation of the exosphere and on the photo-ionisation efficiency. At the subsolar point the ions are generated mainly by photo-ionisation; conversely, in the areas of solar wind access the ion-sputtering ionised component is likely to be the dominant ion source.

3.3.2. *Acceleration, Circulation and Precipitation on the Surface*

The ions drift with velocities determined by the configuration of the magnetic and electric fields. The electric drift is the same for all ions, while the magnetic drift depends on the ion velocity. The Hermean magnetosphere differs from the terrestrial one in two essential respects: boundary conditions and characteristic scales of field variations (see reviews by Russel *et al*., 1988; Wurz and Blomberg, 2001).

Because the dayside magnetopause is located much closer to the planet, an open flux region is expected at Mercury that extends toward latitudes significantly lower than at Earth and allows impacts of accelerated magnetosheath populations over wide portions of the planet surface at medium-high latitudes (see previous section). The proximity of the dayside magnetopause also raises questions about the existence of stable particle trapping near the equatorial plane, and consequently about the possibility of a viable ring current. Though repeated enhancements of the energetic electron flux recorded by Mariner-10 (mentioned before) may be interpreted as signatures of drift echoes (e.g. Baker *et al*., 1986), several quantitative studies of charged-particle dynamics do not show compelling evidence of such closed

drift paths (e.g. Lukyanov *et al*., 2001b; Orsini *et al*., 2001; Delcourt *et al*., 2003; Kallio and Janhunen, 2003a; Mura *et al*., 2004). Moreover, as suggested by Moore *et al*. (2001), the development of a significant ring current, and hence of magnetic storms, may be hampered by a reduced internal plasma source. At the opposite end, boundary conditions near the planet surface also differ from those prevailing at Earth because of the absence of an ionosphere. The various processes that have been proposed for magnetospheric current closure at low altitudes, such as closure through the planet crust or via photo-electron cloud or plasma polarisation (e.g. Glassmeier, 1997), remain highly speculative to date.

From both spatial and temporal viewpoints, the scales of field variations at Mercury are also widely different from those at Earth (as illustrated in Section 3.2). A first straightforward consequence of smaller scale lengths at Mercury is related to the centrifugal acceleration that affects the charged particles during their magnetospheric transport (Delcourt *et al*., 2002). Indeed, for a given propagation speed, the smaller the magnetospheric obstacle is to the expanding solar wind, the larger is the centrifugal acceleration during convection from high to low latitudes. Accordingly, particles of either solar wind or planetary origin, while travelling from high to low latitudes, are subjected to enhanced outward oriented aligned acceleration due to the large curvature of the $\mathbf{E}\times\mathbf{B}$ drift paths, this acceleration yields populations in the magnetospheric lobes that are significantly more energetic (a few hundreds of eVs) than at Earth. For example, Figure 11 shows the energy resulting from three-dimensional trajectory computations for sodium ions from a model exosphere.

Another consequence of small-scale length of field variations at Mercury has to do with the breaking of adiabaticity, which mostly affects those ion species with large mass-to-charge ratios which are sputtered from the planet surface. First order estimates reveal that, in contrast to the Earth's magnetosphere where non-adiabatic transport is expected to occur beyond the nearly dipolar region that extends within about 6 planetary radii, non-adiabatic behaviours may affect the nearby area of Mercury, greater than 2–3 R_M (Delcourt *et al*., 2003). The adiabatic or non-adiabatic character of particle transport is of paramount importance for the magnetosphere structure and dynamics, allowing for particle isotropization and injection inside the loss cone as well as thin current sheet formation (via coherent bunching in gyration phase) or dissipation (via pitch angle scattering). In this regard, randomisation of the ion motion in the innermost magnetosphere is another reason that argues against a stable ring current at Mercury. In fact, Mura *et al*. (2004) show that the protons, at energies above 1 keV, can start to bounce in the dayside magnetosphere, hence being partially trapped, while drifting clockwise (Figure 10, Panel D). Nevertheless, even varying the solar wind conditions, they produce only a partial current around the planet.

A non-adiabatic regime, which is of particular importance is obtained upon resonance between fast oscillations about the tail mid-plane and the slow gyro-motion due to the small normal component of the magnetic field. This quasi-adiabatic

behaviour (Speiser, 1965), that occurs as close as the mid-tail during the growth phase of substorms in the terrestrial magnetosphere (Mitchell *et al*., 1990), may be effective over most of the Hermean magnetotail. The large westward drifts achieved along such orbits occur on scale lengths comparable to that of the magnetotail, leading to prominent ion loss into the dusk flank as well as significant (several keVs) energization in the near-Mercury tail and thin current sheets that extend through most of the nightside sector. Conversely, only ions that circulate in the innermost Hermean magnetosphere (typically within 3 planetary radii for heavy ions) are susceptible to gaining access to the dayside sector, a significant fraction of them being precipitated onto the planet surface because of pitch angle scattering into the wide loss cone.

Figure 12 shows the map of precipitating Na^+. A striking feature on this map is the existence of two bands of intense ($\sim 10^6$ s^{-1} cm^2) impacts of energetic (several keVs) Na^+, which extend over 10° to 20° at mid-latitudes (30°–40°). Whereas the equator-ward boundary of these bands coincides with the edge of the dipolar region, the pole-ward boundary corresponds to the first quasi-adiabatic oscillations in the near-tail, beyond which ions are lost at the dusk magnetopause. These results also corroborate earlier studies that suggested a possible exospheric component due to the planetary energetic ion precipitation (e.g., Potter and Morgan, 1990; Ip, 1993) (see Section 4) and a component of energetic neutral generated via charge-exchange escaping from the planet (Orsini *et al.*, 2001; Barabash *et al*., 2001) (see Section 3.4).

In particular, it may be speculated that, during events of enhanced coupling between the magnetosphere and the solar wind, an increased convection rate will lead to further ion confinement and energization.

Above the magnetosphere on the dayside or on the flanks, the magnetospheric ions could be captured along their large gyroradius from the solar wind ("pick-up ions"), accelerated up to keVs and convected again with the solar wind to the planet (Cheng *et al*., 1987).

The adiabaticity is more applicable when the protons (of solar wind origin) are considered. Orsini *et al*. (2001) and Lukyanov *et al*. (2001b) estimated their distributions inside the magnetosphere in a "scaled" Earth's magnetosphere. Simulations of the solar wind circulation seem to predict another process able to induce a precipitation to the surface. The large gyroradius in the weak magnetic field of Mercury permits the protons to cross the magnetopause and reach the dayside lower latitudes (Kallio and Janhunen, 2004), while precipitations in the nightside high latitudes due to large gyroradii are foreseen by Ip (1997).

Measurements of ion velocity distributions at BC/MPO altitudes will allow the estimation of the drifts in an altitude range where ion trajectories are still adiabatic to a large extent and will allow the characterization of the various regions created by the convection regime. These measurements together with measurements performed at higher distances from the BC/MMO orbit, will furnish a well displayed picture of the ion distribution and circulation in the Hermean environments.

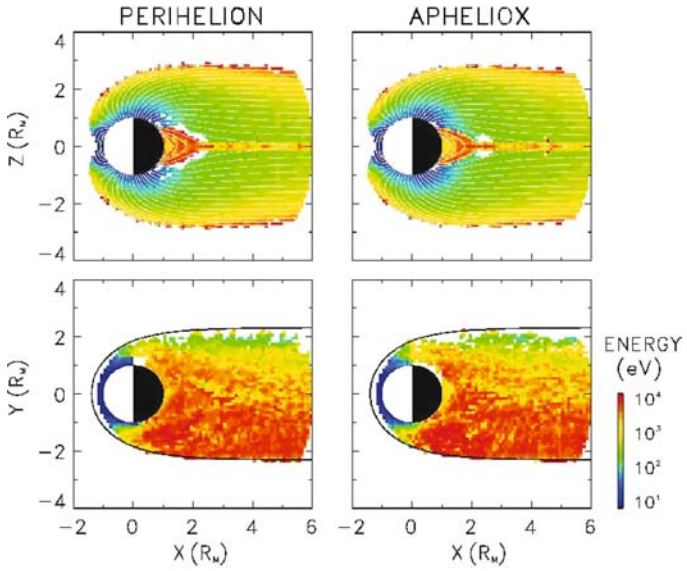

Figure 11. Model average energy of Na^+ ions at (left) perihelion and (right) aphelion. Top and bottom panels show cross-sections in the noon-midnight meridian plane and the equatorial plane, respectively. The energy is coded according to the colour scale at the right (Delcourt *et al.*, 2003).

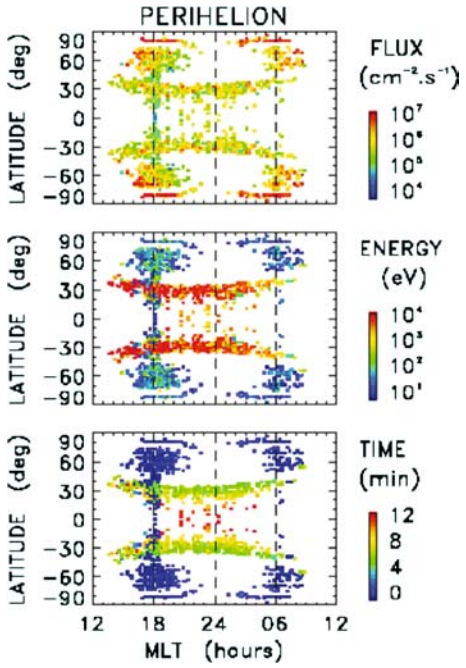

Figure 12. Characteristics of precipitating Na^+ ions at perihelion. The panels from top to bottom show the colour-coded ion flux, average energy, and residence time in the magnetosphere (Delcourt *et al.*, 2003).

3.4. Charge-Exchange ENA Production

The ENAs are produced through charge-exchange between singly charged energetic ions and cold neutrals. The charge-exchange is a symmetrical resonance process in the case of an H^+ projectile and an H target (Hasted, 1964), and could be an accidental resonance process in the cases of different species (for example, O target (Stebbings *et al.*, 1964) and H_2 target (Hasted, 1964)). Hence, in these cases, only a few eV are lost in this interaction, and the newly created ENA retains approximately both the energy of the colliding energetic ion and its direction. At any location, the differential ENA flux, f_{ENA}, generated along a space unit is obtained from the neutral density n by the ion differential flux, f_{ion}, by the charge-exchange cross section σ, and it is a function of energy e, position, and direction $\mathbf{u}$. The newly created ENA, no more affected by magnetic or electric fields, travels in ballistic orbits, i.e. straight lines at keV energies. If its mean free path is long enough, such an ENA can transport information out of the generation region, thus allowing remote sensing of the interaction process (e.g. Roelof *et al.*, 1985; Roelof, 1987; Daglis and Livi, 1995; Orsini and Milillo, 1999; Barabash *et al.*, 2001; Milillo and Orsini, 2001; Orsini *et al.*, 2001).

The differential ENA flux arriving at a vantage point $\mathbf{r}$ is the integral of the ENAs generated along the line of sight $\mathbf{l}$:

$$f_{\mathrm{ENA}}(r, e, u) = \int_{l=0}^{l=\infty} f_{\mathrm{ion}}(r - ul, e, u) \sum_k \sigma_k n_k(r - ul)\, dl \tag{2}$$

where the summation is done for all the neutral species involved in the charge-exchange process.

Hence, the information about the originating ions is transported by ENA away from the ion location. ENAs are indeed carriers of the hot plasma properties. These properties can be obtained through unfolding of the line-of-sight integral f_{ENA}, thus providing an integral estimate of the ion flux distributions as observed from the vantage-point location.

3.4.1. *Imaging of the Plasma via Charge-Exchange ENA and Image Deconvolution*

As stated before (Section 3.2), in the Hermean environment the solar wind ions precipitating toward the planet, at the dayside (e.g. Killen *et al.*, 2001; Kallio and Janhunen, 2003b; Massetti *et al.*, 2003), as well as the protons circulating inside the magnetosphere (Ip, 1997; Lukyanov *et al.*, 2001a; 2001b; Orsini *et al.*, 2001, Mura *et al.*, 2004) could interact with the exospheric atoms via charge-exchange, hence producing a Hydrogen-ENA signal in the energy range of several hundreds of eV and tens of keV. The time scale of emission of such signals is the same as the magnetospheric variation (i.e.: $\approx$1 min.), hence the ENA signal could be seen as localised bursts.

For an Earth-like planetary environment, Orsini *et al*. (2001) and Barabash *et al*. (2001) estimated a differential H-ENA flux emitted from the nightside near equatorial region being up to 10^4–10^5 $(\mathrm{cm}^2\ \mathrm{s\ sr\ keV})^{-1}$. Recently, Mura *et al*. (2004) simulated the ENA signal due to the cusp entered protons. They predicted a strong ENA emission (10^5–10^6 $(\mathrm{cm}^2\ \mathrm{s\ sr})^{-1}$) from the morning side of the planet toward nightside. This signal is more intense when the line of sight is directed toward the tangential view of the planet, since the integrated column is longer and because the bulk of the neutral atmosphere is close to the planet.

Heavier energetic neutrals can be generated via charge-exchange between circulating O^+ or Na^+ and exospheric neutral, however, the signal would be less intense and less focused since the process in this case could be no more resonant.

The instrumentation on board the BC/MPO and BC/MMO spacecrafts will collect ENA images of the planet environment (see Section 5).

Generally, the deconvolution of the ENA images to three-dimensional plasma distributions is not straightforward, since the neutral profile as well as the ion fluxes along the line of sight need to be known. For the Hermean environment, the ENA generation region is quite thin in altitude, and the necessary information on the exospheric density profile as well as the plasma precipitation will be obtained by other instruments on board the same spacecraft (Section 5). Hence, the unfolding procedure will be feasible and useful information on the magnetospheric-exospheric interaction will be obtained by the next mission observations.

4. Exosphere-Surface Interaction

4.1. Mercury's Evolution and Crust Composition Signature

A comparison of uncompressed densities among the Solar System bodies (see Section 1.1) shows that Mercury's interior consists only of a thin mantle and an extremely large iron core with a radius of 70 to 80% of the whole planet (Lewis, 1988). The observed densities of the planets attest to the preservation of primordial differences. The "off-scale" density of Mercury is therefore an indication of either different accretion processes or the presence of an inhomogeneous distribution of elements close to the Sun. Three different formation and evolution scenarios explaining the unusual properties of Mercury (e.g. the high density, the large core, the large Fe/Si ratio among others) are currently discussed in the scientific community:

i. Chemical heterogeneity in the early proto-solar nebula.
ii. The young and hot Sun sublimated and/or vapourised the outer silicate layer.
iii. A giant impact removed the outer silicate layer.

At present, the observational data (see Section 2) are too scarce to help settle on which is the correct scenario, if any. However, a significantly different chemical composition of the mantle will result from each of these three formation

mechanisms. For example, model calculations show that distinctive chemical differences can be expected if planetary vapourisation or a giant impact were responsible for Mercury's present state (Cameron *et al*., 1988). The composition of the surface will reflect the composition of the crust since model calculations show that the "contamination" of the surface by in-fall of meteoritic material is a few percent at most (Küppers, 2004). Detailed knowledge of the chemical composition of the surface and, due to the strict surface/exosphere link, of the exosphere, achievable by instrumentation on board the MESSENGER and BepiColombo missions, would assist the acquisition of information about the early evolution of the planet.

4.1.1. *Chemical Gradient and Heterogeneous Accretion*

The simple equilibrium condensation model for the terrestrial planets accounts approximately for their densities and volatile abundances (Lewis, 1972; Palme, 2000). In this model, as a hot gaseous nebula cools slowly enough for chemical equilibrium to be maintained, a radial compositional gradient results from the thermal gradient (Cassen, 2001). Close to the Sun where temperatures are high, only refractory materials can condense initially, whereas at larger radial distances more volatile elements can also condense. These solids then accrete with little radial mixing to form the terrestrial planets. A secondary result of the gradient in volatile element abundances is that the oxidation state of the material is also a function of radial distance – material condensing close to the Sun is expected to be more reduced than material further out. This model predicts that bulk Mercury should be iron rich, volatile poor, and highly reduced. These conditions favour the large iron core inferred from the planet's high uncompressed density and would result in the formation of silicate minerals low in iron, consistent with observations of the crust. A highly refractory composition would not be expected to give rise to the observations of volatile elements such as potassium and sodium in the exosphere, and the mantle and crust would be expected to have super-chondritic abundances of refractory elements. Furthermore, the lack of volatile light elements means that such a core would be expected to have frozen by now, making the observed magnetic field hard to explain (Conzelmann and Spohn, 1999).

4.1.2. *The Young Sun*

The young Sun may have undergone highly active phases during the first million or even the first 100 million years. Since Mercury is located so close to the Sun, it will have suffered from these initially harsh conditions the most of all planets in the solar system (Bullen, 1952; Cameron, 1985; 1988; Fegley and Cameron, 1987). Standard stellar evolutionary models constructed for the Sun, show that the Zero-Age Main Sequence (ZAMS) Sun, some 4.6 Gyr ago, was about 200 K cooler and about 10% smaller than today, resulting in a luminosity of about 70% of the present Sun. So that in the early stages of the Solar System the young Sun's irradiance is expected to be significantly diminished. The lower luminosity of the young Sun

should therefore have led to a much cooler Earth in the past. However, geological and fossil evidence indicate that the Earth's climate 3–4 Gyr ago and also Mars early climate was not significantly cooler than today and by most geological records probably warmer. This problem has become known as the Faint Young Sun Paradox (FYSP) (Sackmann and Boothroyd, 2002).

Mass-losing solar models which are consistent with helio-seismology can overcome this problem and yield an initial solar mass between 1.03 to 1.07 M_{Sun} (Sackmann and Boothroyd, 2002). Such considerations are recently supported by HST-observations of HI Ly-α absorption lines from the region where the stellar winds of young solar-like stars collide with the interstellar medium. A higher luminosity would have resulted additionally to high sputter rates to an average higher surface temperature and hence, sublimation would have been effective. If this process went on for million of years, the consequence would be a depletion of the surface volatile elements.

In addition to the high mass-loss rates of young solar-like stars, observations also indicate that our young Sun had continuous flare events and the radiation environment was several hundred times more intense than today. The high radiation levels of the young Sun were triggered by strong magnetic activity. The magnetic activity of the Sun is expected to have greatly decreased with time (Guinan *et al*., 2001) as the solar rotation slowed down through angular momentum loss.

Higher XUV and FUV would have caused increased photo-ionisation of atmospheres with the resulting ions efficiently removed by the solar wind. The solar wind, three orders of magnitude larger than today, would have removed any atmosphere of Mercury in a short time.

By studying Mercury one can investigate the possibility that such an early active Sun was responsible for enhanced sublimation processes and blow off of Mercury's silicates (Weidenschilling, 1978). Heating of Mercury by an active Sun (either directly by radiation or by electromagnetic induction) should have greatly depleted volatile elements (including alkali metals) and enhanced refractory elements. The modern crust would have resulted from partial or total melting of the remaining mantle.

4.1.3. *Giant Impact*

In the current planet formation paradigm, the growth of solar system bodies has advanced by means of collisions, first between dust grains and later between larger and larger objects, increasing considerably the relative velocities between colliding bodies (e.g. Wetherill and Stewart, 1989; Cuzzi *et al*., 1993; Weidenschilling *et al*., 1997; Benz, 2000; Inaba *et al*., 2001). This process culminates during the last phases when planet-sized bodies collide at high velocities (e.g. Wetherill, 1988). The high density of planet Mercury can be explained as a consequence of a giant impact (Benz *et al*., 1988; Cameron *et al*., 1988). In this case, a hypothetical differentiated proto-Mercury of chondritic composition (roughly 2.25 times the present mass of Mercury) has been hit by a body 1/6 its mass. The final composition of Mercury

depends upon subsequent re-accumulation of all or parts of the ejected mantle still on Mercury crossing orbits (Benz *et al*., 1988; Tonks *et al*., 1990).

Such dramatic thermodynamical conditions leave detailed chemical and isotopic signatures that, if observable, would provide definitive proof of the giant impact hypothesis and thereby of the entire collisional accumulation paradigm (e.g. Lammer *et al*., 2000). In particular, the overall oxidation state would be unchanged and highly volatile elements are expected to be depleted but with little enhancement of refractory material. If the impact occurred after initial crust formation then many refractory elements such as calcium, aluminium and uranium which preferentially partition into crustal rocks would be lost with the crust, and so the remaining material would not be greatly enhanced in refractory elements despite the high-temperature process (Solomon *et al*., 2001). The abundance of iron oxide would not change greatly, and should reflect the accretion process.

4.2. Crust Composition

The three models proposed to account for Mercury's large uncompressed density (see Section 4.1) differ mainly in the predicted proportions of volatile and refractory elements in the bulk material. Key rock-forming elements include iron, calcium, magnesium, aluminium, titanium, the alkali metals and sulphur.

The first model would result in a regolith enhanced in refractory oxides such as TiO_2, contrary to the evidence cited below. The second model would probably also result in a refractory regolith. A giant impact would result in the loss of much of the silicate portion of the planet. A range of possible compositions for the upper crust was outlined by Goettel (1988), which he called volatile-rich, refractory-rich and preferred, respectively. These are reproduced in Table IV, in part because they have been widely used as the bounds in the literature.

Although the infrared spectra are consistent with a highly reduced surface (e.g. Vilas, 1985), the composition of the exosphere (e.g. Morgan and Killen, 1997), and the presence of an intrinsic magnetic field seem to require a more volatile-rich planet. However, Potter (1995) suggests that if the sodium in the exosphere results from chemical sputtering, then the volatile yield to the atmosphere is greater than previously proposed, and the surface composition need not be as volatile as suggested by Killen *et al*. (1990). At the same time, a lack of metallic iron at the surface must be reconciled with the apparently large iron core and the presence of a magnetic field.

4.3. Surface Elements Release Processes

Loss of volatiles occurs on airless bodies including the Moon, Mercury, and planetary satellites by processes such as impact vapourisation, photon-sputtering (or PSD), thermal desorption, and ion sputtering, followed by Jeans escape or ionisation

TABLE IV
Composition of Mercury, wt. %

	Extreme Refractory-Rich Model	Preferred Model	Extreme Volatile-Rich Model
		Mantle	
Al_2O_3	16.62	3.5–7	3.26
CaO	15.19	3.5–7	3.03
TiO_2	0.72	0.15–0.3	0.14
MgO	34.58	32–38	32.06
SiO	32.58	38–48	45.04
FeO	0	0.5–5	15.07
Na_2O	0	0.2–1	1.40
H_2O	0	a little	a lot
		Core	
Fe	92.48	88–91	76.22
Ni	7.52	6.5–7.5	6.20
S	0	0.5–5	17.58

and entrainment in the solar wind (e.g. Killen *et al*., 2001; Johnson, 2002). The rate of space weathering by evapouration, ion and photon-sputtering is much higher at Mercury (by up to a factor of 10).

4.3.1. *Photon-Stimulated Desorption*

The PSD refers to the desorption of neutrals or ions as a result of direct excitation of a surface atom via a photon. Yakshinskiy and Madey (1999) found in laboratory studies that Na atoms can be released via PSD from surfaces that simulate lunar silicates. They found that bombardment of such surfaces at temperatures of about 250 K by ultraviolet photons with wavelengths 300 nm and below causes very efficient desorption of Na atoms. It was found that the PSD is induced by electronic excitations rather than by thermal processes or momentum transfer. Electron-stimulated desorption (ESD) is less effective but acts in a similar way with a similar threshold. Neutrals are the dominant ejecta. Yields for ions are an order of magnitude lower than for neutrals and exhibit higher thresholds (near 100 and 530 eV). BSD and PSD yields are non-stoichiometric with respect to the surface composition, and principally deplete the most volatile species, mainly Na and K. Water may also be released by PSD and possibly sulphur. Thus, PSD is highly discriminative in reproducing the composition of the surface inside the exosphere. This is because the PSD (and BSD) processes are not energetic enough to remove the more tightly bound atoms.

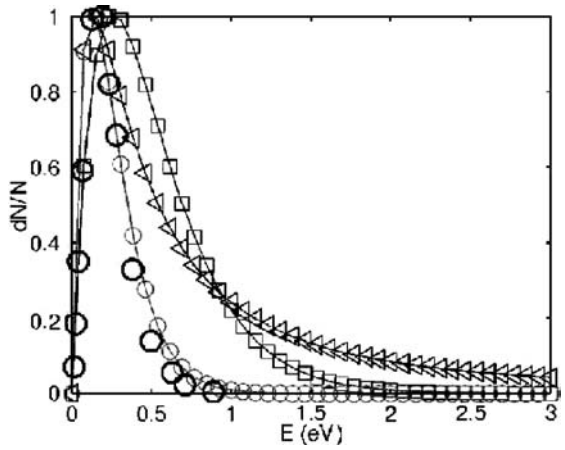

Figure 13. Energy distribution of sodium atoms released from Mercury's surface normalised by its maximum. Square line: micrometeoroid vapourisation. Triangle line: solar wind sputtering. Circle line: photo-stimulated desorption. Dark circle symbols: measurements of Yakshinskiy and Madey (1999). (Leblanc and Johnson, 2003).

In Figure 13 the normalised energy distributions of the sodium atoms ejected via photon sputtering are shown and compared to those obtained via micrometeoroid vapourisation and ion sputtering.

The intensity of the flux of ejected particles varies, of course, with respect to the photon flux at Mercury orbit and therefore scaled to the square of heliocentric distance. At the dayside surface, it depends on the cosine of the zenith angle (there isn't any photon flux at nightside). The rate of ejection of atoms from Mercury's surface can be estimated as the product of UV flux for photon energies >5 eV (Yakshinskiy and Madey, 1999; Killen *et al.*, 2001) times the cosine of the zenith angle, the PSD cross section, which is for sodium $Q_{\mathrm{Na}} \approx 1-3\ 10^{-20}$ cm^2 (Yakshinskiy and Madey, 1999), and the concentration c (surface density by atom fraction). Hence, for constant concentrations over the planetary surface, the largest PSD fluxes of Na occur near equatorial altitudes at perihelion (see Figure 14). In the same time, there should be no noticeable PSD sources at Mercury's polar areas. Conversely, Leblanc and Johnson (2003) hypothesised that, since the subsolar region is depleted in Na atoms, the surface release (PSD and ion sputtering) rates are considerably reduced. Hence, the total rate of ejection of new Na atoms into Mercury's exosphere from Mercury's surface is mainly related to the speed with which the surfaces which were on the nightside come to the dayside. This speed is much higher at the aphelion than at the perihelion and therefore they suggest as a consequence, a larger number of Na atoms in Mercury's exosphere at the aphelion.

Wurz and Lammer (2003) estimated the surface-averaged flux of PSD Na atoms $\approx 4\ 10^{12}$ m^{-2} s^{-1}, with an average release velocity of $v = 890$ m/s, corresponding to 1,100 K, they get a surface density of $n = 7.7$–10^9 m^{-3} in accordance

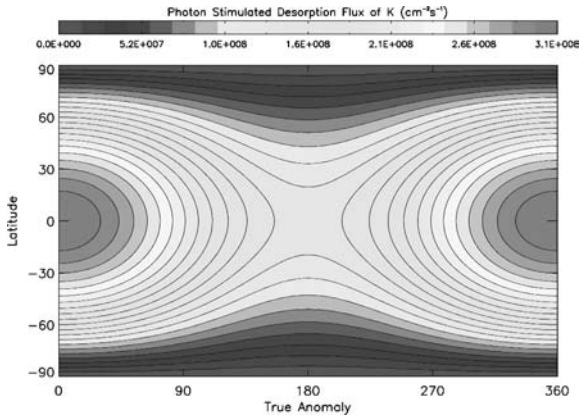

Figure 14. Variation of the photon stimulated desorption flux of Na atoms as function of latitude from the Sun-orientated point on Mercury's surface over its entire orbit (Lammer *et al*., 2003).

with the estimation of $2.1 \cdot 10^{10}$ m^{-3} made by column density measurement of $n_c = 2 \cdot 10^{15}$ m^{-2} of Killen and Ip (1999), by assuming a temperature $T = 1100$ K (sub-solar point). Lammer *et al.* (2003) estimated maximum PSD fluxes $\approx$l–$5 \cdot 10^{10}$ m^{-2} s^{-1}, while McGrath *et al*. (1986) obtained an estimation of $\approx 2 \cdot 10^{11}$ m^{-2} s^{-1} to $2 \cdot 10^{12}$ m^{-2} s^{-1} (probably optimistic since it is based on data for alkali halides (Killen and Morgan, 1993)) and Killen and Morgan (1993) estimated an average Na PSD flux value of $\approx 2.0 \cdot 10^{9}$ m^{-2} s^{-1}. Shemansky and Morgan (1991) estimated a lower Na PSD flux of about $4 \cdot 10^{8}$ m^{-2} s^{-1}.

4.3.2. *Thermal Desorption*

Thermal desorption (TD) is due to the atoms thermal energy exceeding the binding energy at the surface. As for the PSD, the TD depends strongly on the Sun's irradiance, hence the higher TD rate is at subsolar point at perihelion. Yakshinskiy and Madey (1999) studied the Na desorption from a SiO_2 film. They found that the temperature profile of the Na desorption rates strongly depends on the surface composition and structure. Na achieves appreciable desorption rates at a temperature $>$350 K for an Na multilayer. Furthermore, the effect of prolonged bombardment with energetic ions is to shift the desorption peak at higher energy ($>$700 K, see Figure 15).

The TD produces 0.03–0.05 eV sodium atoms (Yakshinskiy and Madey, 2000), whereas the escape energy for Na from Mercury's surface is 2.07 eV. Hence, the desorbed atoms remain close to the surface and do not contribute significantly to planetary loss. However, Hunten and Sprague (1997, 2002) suggested that TD could deplete the sodium surface causing a limitation in other release process rates. Killen and Morgan (1993) suggested that TD, acting over geologic time scales, would serve to deplete the equatorial region of alkalis, moving them pole-ward.

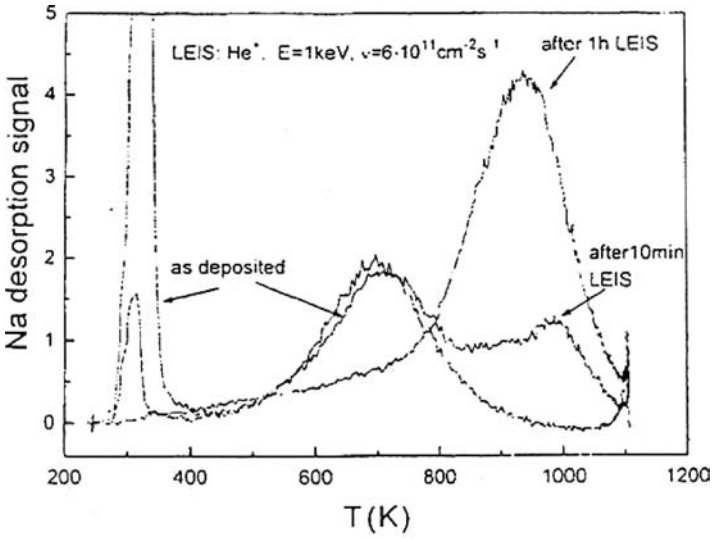

Figure 15. Thermal desorption spectra for desorption of Na from SiO_2 film showing the effect of prolonged bombardment with 1 keV He^+ ions (Madey *et al.*, 1998).

4.3.3. *Ion Sputtering*

In environments where energetic atomic or ionised particles impinge upon a planetary surface, emission of atoms or ions results via sputtering. The energy distribution for sputtered particles, $F(E_e)$, with ejection energy E_e, can be expressed as (Sieveka and Johnson, 1984):

$$F(E_e) \sim \frac{E_e}{(E_e + E_b)^3} \left[1 - \sqrt{\frac{E_e + E_b}{E_i}} \right] \tag{3}$$

in normalised form where E_i is the energy of the incident particle and E_b is the surface binding energy of the sputtered particle. The products arising from this particle bombardment depend both on the composition and chemical structure of the planet surface. A more oxidised surface will result in a higher sputtered-ion content. The positive and negative ion yields are in the range of 0.001 to 0.1 compared to the neutral sputtered fraction.

Since sodium is likely bound to oxygen (oxide composites), the binding energy could be assumed to be 2 eV (McGrath *et al.*, 1986; Cheng *et al.*, 1987). Furthermore, the overall binding energy for oxygen could be estimated as 3–4 eV (Lammer and Bauer, 1997). As an example, the $F(E_e)$ as a function of ejected Na and O particle energy E_e in the case of $E_i = 1$ keV solar wind protons is shown in Figure 16. Wiens *et al.* (1997) measured the velocity distribution from Na_2SO_4 pressed-powder samples by laboratory test. They found that the distribution of

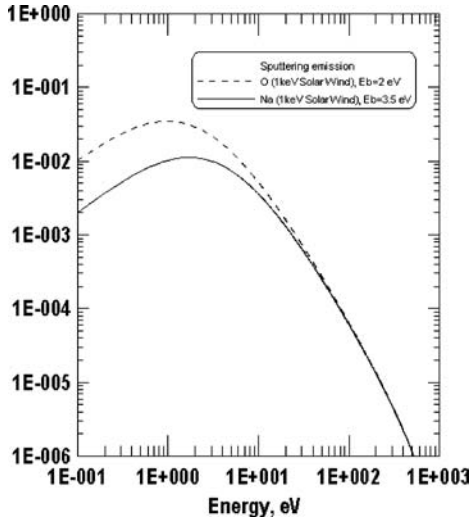

Figure 16. The energy distribution for sputtered particles, $F(E_e)$, as a function of ejected Na and O particle energy E_e in the case of $E_i = 1$ keV solar wind protons.

sputtered particles peaks at 1.5 km/s for Na (and at 1.2 km/s for S). Using the Sigmund-Thomson sputter distribution formula

$$F(E_e) = 2E_b \frac{E_e}{(E_e + E_b)^3} \tag{4}$$

one finds that this distribution peaks at $E_b/2$. Thus, the resulting binding energy is 0.54 eV for Na (and 0.48 eV for S). This reduces (by less then one order in magnitude for Na) the relative intensity of the high energy tail (Figure 13).

Ion sputtering has been suggested as the source of rapid variations in Mercury's sodium exosphere (Potter and Morgan, 1990; Killen *et al*., 2001). Furthermore, Lammer and Bauer (1997) showed that solar wind sputtering is able to explain the observation of a high-altitude sub-solar non-thermal Na exosphere (Potter *et al*., 2002a). In the Hermean environment, the ions precipitating on the surface could be of solar wind origin or ions from the Hermean magnetosphere (see Section 3.3).

Many studies tried to estimate the solar wind particle flux impacting on the surface through the cusps and the location and extension of such a precipitation (e.g., McGrath *et al*., 1986; Sieveka and Johnson, 1984; Cheng *et al*., 1987; Johnson, 1990; Lammer and Bauer, 1997; Killen *et al*., 2001; Kallio and Janhunen, 2003b; Massetti *et al*., 2003). Recently, the resulting sputtered Na and O have been estimated by Massetti *et al*. (2003) and are presented in Figure 17.

An additional "secondary" source of ion sputtering could occur where the ions circulating inside the magnetosphere precipitate onto the surface. These ions could originate from the planet or could come from the solar wind after being mirrored back in the cusp regions. Ip (1993) examined the spatial distribution of the

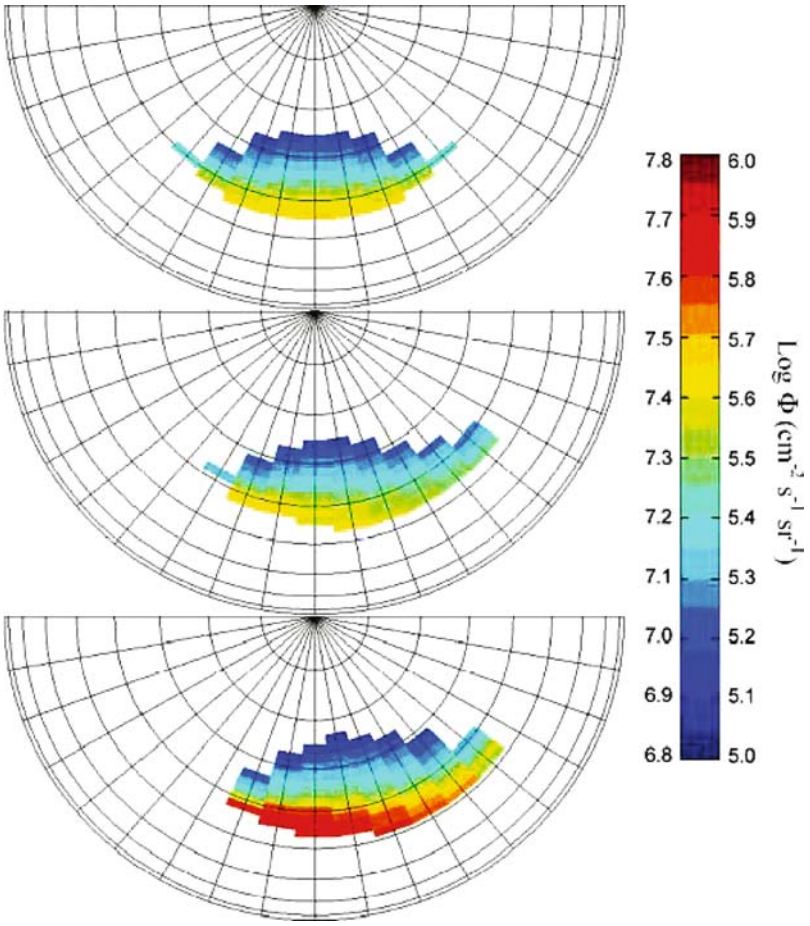

Figure 17. Colour-coded Na-ENA (right scale) and O-ENA (left scale) flux spatial distribution generated by ion-sputtering from the open magnetic field area on the northern dayside surface of Mercury. The three panels refer to different solar wind conditions $P_{\rm dyn} = 16$ nPa, $B_y = 0$ nT and $B_z = -10$ nT (top panel), $P_{\rm dyn} = 16$ nPa, $B_y = -5$ nT and $B_z = -10$ nT (middle panel), $P_{\rm dyn} = 60$ nPa, $B_y = -5$ nT and $B_z = -10$ nT (bottom panel) (Massetti *et al.*, 2003).

precipitating ion flux as a function of local time and latitude for different energies. He concluded that the low-energy (<1 keV) ions preferentially impact at high latitude on the nightside in the predawn sector, and the high-energy (>10 keV) ions preferentially impact the nightside hemisphere at low latitudes. The extended sodium neutral atom tail discovered by Potter *et al.* (2002a) can possibly be explained by sputtering from the nightside of the planet. Delcourt *et al.* (2003) simulated the Na^+ circulation in the Hermean magnetosphere (see Section 3.3) and estimated the sputtered Na generated by Na^+ impacting on the planetary surface. Figure 18 shows the sputtered Na atoms caused by precipitation Na^+ ions at perihelion in three energy ranges. The flux of sputtered Na atoms is 3 to 4 orders of

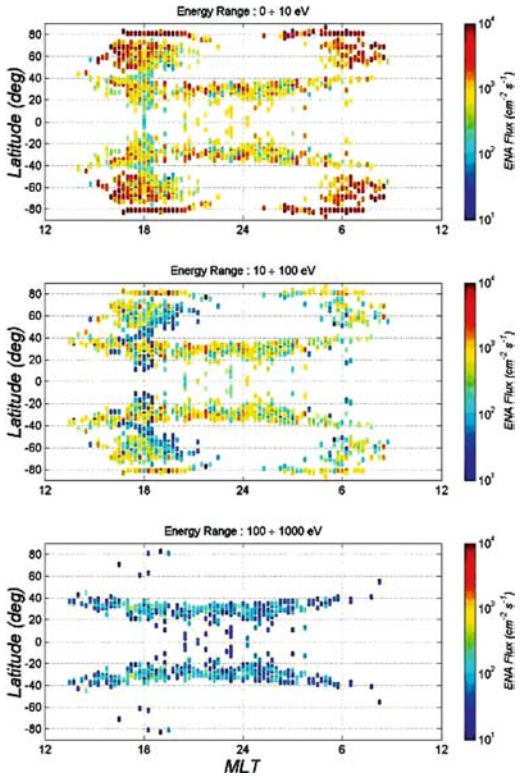

Figure 18. Flux of sodium atoms due to Na^+ ions precipitating from the magnetosphere at perihelion. The neutral atom flux is shown in the three different energy ranges (0–10 eV, 10–100 eV, 100–1000 eV) (Delcourt *et al.*, 2003).

magnitude smaller than the flux due to precipitating solar wind protons (e.g. Massetti *et al.*, 2003). However, the sputtering directly induced by the cusp-precipitating solar wind and that due to energetic magnetospheric ions are effective in quite distinct regions, namely at high latitudes in the dayside sector in the former case and within an extended rim at mid-latitudes in the latter case. A crude estimate of the flow rate in the nightside sector yields 10^{20}–10^{21} s^{-1} only for sodium atoms. Since sodium is only a minor constituent on the surface we estimate the total production of heavy neutrals (e.g. O, Mg, Si, ...) to be in the range of 10^{22}–10^{23} s^{-1}. Hence, sputtering due to ion precipitation from the magnetosphere may play a significant role in refilling of the exosphere and erosion of the planet's surface.

4.3.4. *Micrometeorite Impacts*

In interplanetary space there are micrometeoroids orbiting around the Sun approximately distributed according to an R^{-2} scaling factor (Grün *et al.*, 1980). The

micrometeoroid vapourisation on the planetary surface produces impact flashes, reported to be Maxwellian at about 4,500 K, with a mean velocity of 2 km/s (Sugita *et al*., 1997) (the energy distribution is shown in Figure 13). This source would be energetic enough to produce a comet-like tail at high radiation pressure conditions, hence it could be responsible for the observations of Na D lines at high altitude (Lammer *et al*., 2003). More recently, the velocity distribution of impact ejecta has been found to be a function of the tensile strength of the target material (Onose and Fujiwara, 2003), and the velocity of impact ejecta can be quite low. In addition, the spatial distribution and energy of jets is very dependent on the tensile strength of the target as well as on the impact angle of the projectile. Cremonese *et al*. (2003) in their preliminary model suggest that the kinetic energy of each atom, ejected by micrometeoroid vapourisation, does not depend on the mass of the impacting meteoroid, for a mass range of 1–100 kg of the impactor and an impact velocity greater than 30 km/s. Each atom inside the produced vapour has the same initial kinetic energy distribution; in particular the Na atom energy does not depend on the Na concentration inside the vapourised regolith, assuming that the internal energy of the vapour is equally divided among the different kind of atoms.

The energy of ejected atoms has a maximum for meteorite impact velocities of about 35 km/s. When the meteorite velocity $V_A < 30$ km/s, we can no longer neglect the vapourised mass of the meteorite.

Killen *et al*. (2001) found that impact vapourisation consistently produces only about a quarter of the source flux of sodium to the atmosphere, so that PSD is consistently the dominant source process for their data set.

Vapourisation rates should differ for different elements, but this topic has not been extensively studied (Killen, 2002b). Wurz and Lammer (2003) argued that micrometeoroid impacts contribute especially to exosphere low-volatile and refractory component, and may be the only process for this material at the night side.

Morgan *et al*. (1988) estimated a vapourisation rate for Na atoms of about 0.15–$14 \cdot 10^{23}$ s^{-1}, while Leblanc and Johnson (2003) estimated it at about $3.5 \cdot 10^{23}$ s^{-1}, indicating that the micrometeoroids could contribute up to 30% of the Sodium exosphere. Wurz and Lammer (2003) estimated a released Na flux of about 10^{12} m^{-2} s^{-1}. In any case, these estimates refer to a mean global value that will be much larger when considering each instantaneous meteoroid impact. Micrometeoroid vapourisation is likely to be the most important process for the nightside, unless significant ion sputtering occurs.

4.3.5. *Chemical Sputtering*

Chemical sputtering refers to the release of atoms or molecules from the surface as a result of chemical reactions of implanted solar wind or magnetospheric ions with the surface minerals. Production of molecules on the surface of Mars was considered by Huguenin (1976) and on the surface of Mercury by Gibson (1977). Huguenin (1976) suggested that in addition to the production of water, the OH radical serves to reduce Fe^{2+} to Fe^0, removing O^{2-} from the surface lattice sites.

These processes could potentially explain the low upper limit of O in the Hermean and lunar exospheres, water ice at the poles (Salvail and Fanale, 1994; Paige, 1992; Slade *et al*., 1992), and the absence of Fe^{2+} in the regolith. Potter (1995) proposed that the distribution of Na is consistent with a chemical sputtering source.

5. Exosphere Investigation via Spacecraft Observations: Main Scientific Objectives of the BC/MPO/SERENA Experiment

As mentioned in the previous sections, many instruments in the upcoming missions will be devoted to improving our knowledge of the surface-exosphere-magnetosphere system of Mercury. Among the others, an instrument named SERENA (Search for Exospheric Refilling and Emitted Natural Abundances, see ESA 'BepiColombo Payload Definition Document (FDD)', issue 4, revision 0–19 December 2003) proposed on board the BC/MPO satellite will be dedicated to particle detection. In fact, the interaction between the Hermean environment with energetic plasma particles, solar radiation and micrometeorites gives rise to both thermal and directional neutral populations (via surface release and charge-exchange processes) in the near-planet space; such populations will be recorded by SERENA NPA (Neutral Particle Analyser) and by the ENA imager proposed for BC/MMO. The photo-ionised or charged component of the surface release processes as well as the plasma precipitation and circulation in the Hermean magnetosphere will be recorded by the SERENA IS (Ion Spectrometer), by the particle detectors on board BC/MMO and by the MESSENGER particles and plasma spectrometers (for low and high-energy ions: Livi *et al*. 2003). Remote sensing of many exospheric species will be achieved by the Ultra Violet Spectrometers (UVS) on board BC/MPO and by the UltraViolet-Visible Spectrometer (UVVS) of MESSENGER. The expected observations will help to explain many of the unsolved questions related to the Hermean environment.

Considering that the authors of this review are presently members of the BC/MPO/SERENA NPA& IS-Science Team, in the next sub-sections, the main scientific objectives achievable by this experiment will be outlined in the context of the whole instrumentation devoted to exospheric studies on board of BepiColombo.

5.1. Neutral Exosphere Detection

As described in Section 2.1, the six observed elements constitute only a small fraction of Mercury's exosphere and the analysis of the density and composition of the local exospheric gas directly detected from orbiting satellite is needed.

The thermal neutral particle detector STROFIO of the SERENA NPA experiment will be able to observe and identify molecules, atoms and, possibly, their isotopes. The only limitation for such measurements is the necessary presence with sufficient density of such species at the orbital altitude. Figure 19 shows the exospheric

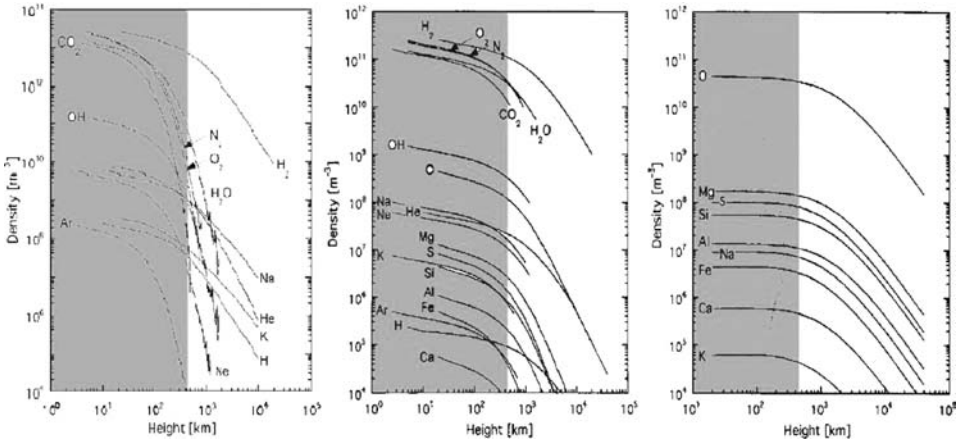

Figure 19. Exospheric densities for thermal emission and PSD for Na and K at the dayside (left panel) for micro-meteoritic impact vapourisation (middle panel) and for ion sputtering (right panel) as computed by Wurz and Lammer (2003). The white sector represents the species present at the BC/MPO orbit.

densities resulting from a Monte-Carlo two-dimensional-exosphere model (Wurz and Lammer, 2003) of different species emitted from the surface by different release processes. In the figure the species at the BC/MPO orbit are evidenced. For PSD and thermal desorption (without considering the radiation pressure which is important mostly for the alkali atoms) (left panel) the spectra are dominated, on the dayside, by volatile components like H_2, H_2O, N_2, O_2 and CO_2. It is probable that those molecules which may be released are quickly dissociated producing an extra signal of atomic Oxygen, however, H, He, Ne, OH, Na, and K will also be detectable. Micro-meteorite impact vapourisation (middle panel) results in different spectra with both volatile and refractory species from the surface. Finally, where sputtering by solar wind ions is the active process, the resulting mass spectra (right panel) are dominated by refractory species. The dayside and nightside altitude profile of the observed elements, between periherm and apoherm (400–1500 km) is derivable with similar detailed information. Moreover, STROFIO will be able to observe asymmetries, induced by strong thermal variations, between day/night, dawn/dusk sides and perihelion/aphelion. A careful study of Oxygen isotopes (probably addressable by STROFIO in specific conditions, see Section 2.1.2) provides insight into the evolutionary history of the Solar System.

Some of the elements mentioned (such as H, O, OH and H_2O) will be observed even by the UVS especially at the dayside, while the heavier atoms, such as N, C, Ne, Si, Ar, Fe, Mg and molecules, will be observed, probably, solely by the UVS since it is unlikely they arrive at the BC/MPO orbit. At the same time, the UVS will provide, only at the dayside, column density profiles along a line-of-sight for many species below the spacecraft orbit.

The combination of these two experiments on BepiColombo could be an unprecedented opportunity to perform a detailed analysis of the exosphere composition and vertical profiles.

More specifically, remote measurements (by instrumentation on board BC/MPO) of Mercury's surface and exosphere, by using X-ray, UV and optical spectroscopy, as well as *in situ* measurements of the exospheric composition using SERENA NPA, will help to explain the cycling of volatile elements between Mercury's interior, surface and exosphere, and the contribution of meteoritic/cometary material and solar wind plasma to Mercury's near-surface volatile budge.

The detailed knowledge of the species distributions around the planet will test the different theories of exospheric refilling and circulation.

Particle release processes – like PSD, election stimulated desorption, thermal desorption and particle-sputtered surface constituents (see Section 4) – depend mainly on the mineralogical and geochemical properties of Mercury's surface, incoming solar UV radiation, X-rays, galactic cosmic ray and energetic solar wind particle exposure. We expect a high-energy component of the exosphere due to release processes such as ion-sputtering (see Section 4) and to charge-exchange processes between energetic charged particles of solar wind/magnetospheric origin with the thermal neutral exospheric component (see Section 3.4). The sensor ELENA of the SERENA NPA experiment will detect only the directional neutral particles, so that it will have the possibility to separate thermal particles, which are released from the surface into Mercury's exosphere via low energetic desorption processes and micrometeorite vapourisation, from the more energetic exospheric particle populations generated via ion-sputtering and charge-exchange processes. Moreover, the SERENA/ELENA unit, complemented by the precipitating plasma observation of the SERENA IS/MIPA instrument, will offer the scientific community for the first time the chance to identify and to localise the different physical processes acting on the surface as well as to estimate their relative efficiencies and to directly observe the spectrum of the high-energy exospheric component lost in space. Since the charge-exchange neutral are mainly Hydrogen while the ion-sputtered neutrals are heavier atoms, the energy analysis of SERENA/ELENA will permit clear discrimination between the active loss process and the preferential starting point of loss.

The ELENA unit of SERENA NPA will be able to obtain an instantaneous ($\cong$1 min of integration time) array of charge-exchange H-ENA with resolution around 2°. The satellite track will furnish the second dimension in the ENA images performed by the unit.

A global-scale high-energy ENA monitor located on the BC/MMO will study the solar wind-magnetosphere interaction, as well as the magnetospheric plasma dynamics. Such investigations will fruitfully complement the exosphere studies performed by SERENA NPA/ELENA, so that a comprehensive picture of the planet's neutral particle environment will be obtained.

Generally, deconvolution of the ENA images is not straightforward, since the neutral profile as well as the ion fluxes along the line of sight could be unknown. In the Hermean condition, the ENA generation region is quite thin (in altitude), and some information on the exospheric density profile will be obtained by the UVS and by the SERENA NPA/STROFIO measurements. Moreover, some info on the plasma precipitation could be obtained from the BC/MMO instrumentation as well as from the measurements performed by BC/MPO/SERENA IS. Hence, the unfolding procedure will be feasible and useful information on the magnetospheric-exospheric interaction will be obtained by these observations.

Furthermore, the comparison of the ENA observations in Mercury's environment with neutral particle images of Earth (IMAGE), Mars (Mars Express), Venus (Venus Express), Jupiter, Saturn and Titan (Cassini) environments will allow comparative investigations of the evolution and dynamics of planetary magnetospheres and atmospheres.

Due to the strong link between the exosphere and the surface, by measuring neutrals and ions at relatively low altitudes SERENA will offer the possibility to get information on the upper surface composition below the cusp regions (e.g. Figure 16 from Massetti *et al*., 2003). Nevertheless, the release processes are non-stoichiometric, so that each process involves preferential species. Hence, taking into account the effectiveness of the process in ejecting material, we can gain information about the surface composition. Furthermore, the flow direction of the neutrals detected by ELENA will allow determination of the surface area (with a resolution of tens of km) from which the particles are escaping. ELENA will permit an accurate determination of the energy distribution of the high-energy tail of ion-sputtered neutral atoms, while STROFIO will measure the composition of the bulk of ion-sputtered neutral atoms. Hence, both these observations will permit remote sensing of the relative upper surface abundances. Furthermore, information on the composition of the bulk regolith can be derived from the total escape rates of atoms and ions by the whole SERENA experiment. This surface composition analysis could help the more specifically devoted observations by X-Ray from MPO.

5.2. Ion Exosphere Detection

The photo-ionised or charged component of the surface release processes as well as the plasma precipitation and circulation in the Hermean magnetosphere will be recorded by the SERENA IS sensors. The UV spectrometer studied for BC/MPO will most probably be very limited in its ability to observe Mercury's exospheric ion emissions because of the low airglow intensity of such ions (see e.g. Phebus: Ultraviolet spectrometer proposal for BC/MPO). The BC/MPO orbit, close to the planet, and the good duty cycle, allowed by 3-axis stabilization, will permit to obtain measurement of the sputtered ions continuously enabling a detailed composition measurement.

Along the BC/MPO orbit at low altitude, the PICAM unit will be able to detect freshly ionised particles. The quantification of the ion component will provide useful information for the unsolved problem of the presence of an exo-ionosphere at Mercury. The high sensitivity, the wide FOV and the mass resolution of PICAM will allow detection of the low-density ion components and completion of the composition analysis of the Hermean envelope. The measurement of the ion velocity distribution for some of the species will provide information on the main mechanisms of acceleration inside Mercury's magnetosphere but also because of the difference in concentration within the exosphere on the main origin of the exospheric neutral particles. The energy distribution will provide key information about the type of ejection mechanisms of their parent neutral atoms.

When BC/MPO is located within the exo-ionosphere or the magnetosphere, ion measurements will provide information about the particles that have drifted while penetrating the magnetosphere. Near the BC/MPO apocentre, and when above the magnetosphere on the dayside or on the flanks, an ion spectrometer will "see" the influence of a significant portion of the magnetosphere on the solar wind ions and on planetary pick-up ions that were captured by the solar wind and convected with the solar wind to the planet. This information, in combination with the data on convection in the Hermean magnetosphere performable by PICAM and MIPA and with correlated measurements performed by the ion spectrometer MSA on board BC/MMO, will help in understanding the structure and dynamics of the magnetosphere of Mercury. The quantification of the ionised component will provide evidence about the possibility of having enough exospheric conductivity, hence, providing crucial information for solving the open question related to the currents closure.

The SERENA IS/MIPA will fruitfully complement the ion-sputtered neutral particle observations of SERENA NPA/ELENA and STROFIO, as stated before, by monitoring the strong solar wind precipitation in the cusp regions. At the same time, SERENA IS/PICAM will detect the low-density signal resulting from the ion-sputtered ionised component. Hence, the joint effort of the four SERENA units will allow an unprecedented detailed analysis of the ion-sputtering process at Mercury.

The high-energy neutral and ion products of the release processes, as well as the charge-exchange ENA, are mainly created close to the surface and carried away from the planetary environment due to Jeans escape and to electromagnetic transport. Such processes produce a global particle loss rate from the planet. The global loss rate can be evaluated by the measurements performed by ELENA, PICAM and MIPA units of SERENA, thus providing crucial information for deriving the past and present evolution of the planet.

In summary, BC/MPO/SERENA NPA – IS is an experiment able to provide information about the whole surface-exosphere-magnetosphere system and the processes involved in the system as well as in the interaction with the solar wind and the interstellar medium.

Acknowledgments

The authors would like to thank Dr. Francois Leblanc for useful comments on this review.

References

Baker, D. N., Simpson, J. A., and Eraker, J. H.: 1986, *J. Geophys. Res.* **91**, 8742.
Balogh, A., Bird, M., Blomberg, L., Bochsler, P., Bougeret, J.-L., Brückner, J. *et al.*: 2000, BepiColombo—An interdisciplinary cornerstone mission to the planet Mercury. *ESA-SCI (2000) 1*, Noordwijk, The Netherlands, European Space Agency.
Barabash, S., Lukyanov, A. V., C:son Brandt, P., and Lundin, R.: 2001, *Planet. Space Sci.* **49**, 1685.
Benz, W.: 2000, *Space Sci. Rev.* **92**(1/2), 279–294.
Benz, W., Slattery, W. L., and Cameron, A. G. W.: 1988, *Icarus* **74**, 516–528.
Bida, T. A., Killen, R. M., and Morgan, T. H.: 2000, *Nature* **404**(9), 159–161.
Bougeret, J. L., King, J. H., and Schwenn, R.: 1984, *Solar Phys.* **90**, 401–412.
Broadfoot, A. L., Shemanky, D. E., and Kumar, S.: 1976, *Geophys. Res. Lett.* **3**, 577.
Bullen, K. E.: 1952, *Nature* **170**, 363–364.
Butler, B. J.: 1997, *J. Geophys. Res. (Planets)* **102**, 19283–19291.
Butler, B. J., and Muhleman, D. O.: 1993, *J. Geophys Res.* **98**, 15003–15023.
Cameron, A. G. W.: 1985, *Icarus* **64**, 285–294.
Cameron, A. G. W.: 1988, *Ann. Rev. Astron. Astrophys.* **26**, 441–472.
Cameron, A. G. W., Benz, W., Fegley, B., and Slattery, W. L.: 1988, The strange density of Mercury – Theoretical considerations, in F. Vilas, C. R. Chapman, and M. S. Matthews (eds.), *Mercury,* Univ. of Arizona Press, Tucson, pp. 692–708.
Cassen, P.: 2001. *Meteorit. Planet. Sci.* **36**, 671–700.
Cheng, A. F., Johnson, R. E., Krimigis, S. M., and Lanzerotti, L. J.: 1987, *Icarus* **71**, 430–440.
Clayton, R. N.: 2003, *Sp. Sci Rev.* 106, 19–32.
Connerney, J. E. P., and Ness, N. F.: 1988, The magnetosphere of Mercury, in F. Vilas, C. R. Chapman, and M. S. Matthews (eds.), *Mercury,* Univ. of Arizona Press, Tucson, p. 494.
Conzelmann, V., and Spohn, T.: 1999, *Proceedings of the DPS, Bull. Am. Astron. Soc.* **31**, 1802.
Cremonese, G., Boehnhardt, H., Crovisier, J., Rauer, H., Fitzsimmons, A., Fulle, M., Licandro, J., Pollacco, D., Tozzi, G. P., West, R. M.: 1997, *Ap. J.* **490**, L199.
Cremonese, G., Orsini, S., Mangano, V., Capria, M. T., Milillo, A., and Mura, A.: 2003, *EGS-AGU-EUG Joint Assembly,* 7–11 April.
Cuzzi, J. N., Dobrovolskis, A. R., and Champney, J. M.: 1993, *Icarus* **106**, 102–134.
Daglis, I. A., and Livi, S.: 1995, *Ann. Geophys.* **13**, 505–516.
Delcourt, D. C., Moore, T. E., Orsini, S., Millilo, A., and Sauvaud, J.-A.: 2002, *Geophys. Res. Lett.* **29**(12), 10.1029/2001GL013829, 32.
Delcourt, D. C., Grimald, S., Leblanc, F., Berthelier, J.-J., Millilo, A., Mura, A. *et al.*: 2003, *Annal. Geophys.* **21**, 1723–1736.
Eraker, J. H., and Simpson, J. A.: 1986, *J. Geophys Res.* **91**, 9973–9993.
Fegley, B., and Cameron, A. G. W.: 1987, *Earth Planet. Sci. Lett.* **82,** 207–222.
Fjelbo, G., Kliore, A., Sweetnam, D., Esposito, P., Seidel, B., and Howard, T.: 1976, *Icarus* **29**, 407–415.
Gibson, E. K., Jr.: 1977, *Phys. Earth Planet. Inter.* **15**, 303–312.
Glassmeier, K.-H.: 1997, *Planet. Space Sci.* **45**, 119–125.

Goettel, K. A.: 1988, Present bounds on the bulk composition of Mercury: Implications for planetary formation processes, in F. Vilas, C. R. Chapman, and M. S. Matthews (eds.), *Mercury,* Univ. of Arizona Press, Tucson, p. 613–621.
Goldstein, B. E., Suess, S. T., and Walker, R. J.: 1981, *J. Geophys. Res.* **86**, 5485–5499.
Gombosi, T. I.: 2000, *Magnetospheric Current System,* AGU Geophysical Monograph **118**, 363–370.
Grün, E., Pailer, N., Fechtig, H., and Kissel, J.: 1980, *Planet. Space Sci.* **28**, 333–349.
Guinan, E. F., Ribas, I., and Harper, G. M.: 2001, Reconstruction the Sun's magnetic history and spectral irradiance evolution from X-ray, EUV, and FUV observations of solar proxies with different ages, *The Evolving Sun and its Influence on Planetary Environments,* Granada, Spain.
Hapke, B.: 1986, *Icarus* **66**, 270.
Harmon, J. K., and Slade, M. A.: 1992, *Science* **258**, 640–642.
Harmon, J. K., Slade, M. A., Velez, R. A., Crespo, A., Dryer, M. J., and Johnson, J. M.: 1994, *Nature* **369**, 213–215.
Harmon, J. K., Perillat, P. J., and Slade, M. A., 2001, *Icarus* **149**, 1–15.
Hasted, G. B.: 1964, *Physics of Atomic Collisions,* Butterworths, London, P. 416.
Hodges, R. R.: 1974, *J. Geophys Res.* **79**, 2881–2285.
Hodges, R. R.: 1975, *Moon* **14**, 139–157.
Hodges, R. R., and Johnson, F. S.: 1968, *J. Geophys Res.* **73**, 7307–7317.
Hodges, R. R., Hoffman, J. H., Johnson, F. S., and Evans, D. E.: 1973, *Proc. Lunar Sci. Conf., 4th*, 2865–2875.
Huebner, W. F., Keady, J. J., and Lyon, S. P.: 1992, *Astrophys. Space Sci.* **195**, 1–294.
Hunten, D. M., and Sprague, A. L.: 1997, *Adv. Space Res.* **19**, 1551–1596.
Hunten, D. M., and Sprague, A. L.: 2002, *Meteoritics Planet. Sci.* **37**, 1191–1196.
Hunten, D. M., Morgan, T. H., and Shemansky, D. E.: 1988, The Mercury atmosphere, in F. Vilas, C. R. Chapman, and M. S. Matthews (eds.), *Mercury,* Univ. of Arizona Press, Tucson, pp. 562–612.
Huguenin: 1976, *Proc. Colloq. on Water in Planetary Regoliths,* pp. 33–43.
Inaba, S., Tanaka, H., Nakazawa, K., Wetherill, G. W., and Kokubo, E.: 2001, *Icarus* **149**, 235–250.
Ingersoll, A. P., Svitek, T., and Murray, B. C.: 1992, *Icarus* **100**, 40–47.
Ip, W.-H.: 1986, *Geophys. Res. Lett.* **13**(5), 423–426.
Ip, W.-H.: 1993, *Astrophys. J.* **418**, 451–456.
Ip, W.-H.: 1997, *Adv. Space Res.,* **19**, 1615–1620.
Ip, W.-H., and Kopp, A.: 2002, *J. Geophys. Res.* **107**, A11, doi:10.1029/2001JA009171, 1348.
Kabin, K., Gombosi, T. I., DeZeeuw, D. L., and Powell, K. G.: 2000, *Icarus* **143**, 397–406.
Kallio, E., and Janhunen, P.: 2003a, *Annales Geophysicae* **21**(11) 2133–2145.
Kallio, E., and Janhunen, P.: 2003b, *Geophys. Res. Letters.* **30**(17), 10.1029/2003GL017842, 1877.
Kallio, E., and Janhunen, P.: 2004, *Adv. Space Res.* **33**(12), 2176–2181.
Killen, R. M.: 2002a, *Meteorit. Planet. Sci.* **37**, 1223–1231.
Killen, R. M.: 2002b, Selective volatile depletion on the surface of asteroids, *Proceedings of the Asteroids, Comets and Meteors Conference* **ESA SP-500,** Berlin, Germany.
Killen, R. M., and Morgan, T. H.: 1993, *Icarus* **101**, 293–312.
Killen, R. M., and Ip, W.-H.: 1999, *Reviews of Geophysics* **37**, 361.
Killen, R. M., Potter, A. E., and Morgan, T. H.: 1990, *Icarus* **85**, 145–167.
Killen, R. M., Benkhoff, J., and Morgan, T. H.: 1997a, *Icarus* **125**, 195–211.
Killen, R. M., Potter, A. E., and Morgan, T. H.: 1997b, *BAAS* **29**(3), 987.
Killen, R. M., Potter, A. E., Fitzsimmons, A., and Morgan, T. H.: 1999, *Planet. Space Sci.* **47**, 1449–1458.
Killen, R. M., Potter, A. E., Reiff, P., Sarantos, M., Jackson, B. V., Hick, P. *et al.* : 2001, *J. Geophys Res.* (*Planets*) **106**, 20,509–20,525.
Killen, R. M., Sarantos, M., and Reiff, P.: 2004a, *Ads. Space Res.* **33**(11), 1899–1904.

Killen, R. M., Bida, T. A., and Morgan, T. H.: 2004b, *Icarus*, in press.
Küppers, M.: 2004., *Icarus*, in press.
Janhunen, P., and Kallio, E.: 2004, *Annales Geophysicae* **22**, 1829–1837.
Johnson, R. E.: 1989, *Icarus* **78**, 206.
Johnson, R. E.: 1990, *Energetic Charged-Particle Interaction with Aatmospheres and Surfaces,* Springer-Verlag, Berlin.
Johnson, R. E.: 2002, Surface boundary layer atmospheres, in M. Mendillo, A. Nagy and J. H. Waite (eds.), *Atmospheres in the Solar System: Comparative Aeronomy,* AGU.
Lammer, H., and Bauer, J.: 1997, *Planet. Space. Sci.* **45**, 73–79.
Lammer, H., Stumptner, W., Molina-Cuberos, G. J., Bauer, S. J., and Owen, T.: 2000, *Plan. Space Sci.* **48**, 529–543.
Lammer, H., Wurz, P., Patel, M. R., Killen, R. M., Kolb, C., Massetti, S. *et al.* : 2003, *Icarus* **166/**2, 10.1016/j.icarus.2003.08.006, 238–247.
Leblanc, F., and Johnson, R. E.: 2003, *Icarus* **164**, 261–281.
Leblanc, F., Delcourt, D., Johnson, R. E., and Liu, M.: 2003, *J. Geophys. Res. Planets,* E12, 10.1029/2003JE002151, 5136.
Leblanc, F., Lammer, H., Torkar, K., Berthelier, J. J., Vaisberg, O., and Woch, J.: 2004. *Notes du Pole de Planetologie de 1'IPSL,* No 5, (http://www.ipsl.jussieu.fr/Documentation).
Lewis, J. S.: 1972, *Earth Planet. Sci. Lett.* **15**, 286–290.
Lewis, J. S.: 1988, Origin and Composition of Mercury, in F. Vilas, C. R. Chapman, and M. S. Matthewsin (eds.), *Mercury,* Univ. of Arizona Press, Tucson, pp. 651–666.
Livi, S. A., McNutt, R., Andrews, G. B., Keath, E., Mitchell, D. G., and Ho, G.: 2003, The energetic particles spectrometers (EPS) on MESSENGER and NEW HORIZON, *AIP Proceedings CP 679 of Solar Wind X Conference*, 838–841.
Luhmann, J. G., Russell, C. T., and Tsyganenko, N. A.: 1998, *J. Geophys. Res.* **103**, 9113–9119.
Lukyanov, A. V., Umnova, O., and Barabash, S.: 2001a, *Plan. Space Sci.* **49**(14–15), 1669–1675.
Lukyanov, A. V., Barabash, S., Lundin, R., and C:son Brandt, P.: 2001b, *Planet. Space Sci.* **49**, 1677.
Lundin, R., Barabash, S., C:son Brandt, P. C., Eliasson, L., Nairn, C. M. C., Norberg, O. *et al.* : 1997, *Ads. Space Res.* **19**, 1593–1607.
Madey, T. E., Yakshinskiy, B. V., Ageev, V. N., and Johnson, R. E.: 1998, *J. Geophys. Res.* **103**, 5873.
Massetti, S., Orsini, S., Milillo, A., Mura, A., De Angelis, E., Lammer, H. *et al.* : 2003, *Icarus* **166**(2), 229–237, 10.1016/j.icarus.2003.08.006.
McGrath, M. A., Johnson, R. E., and Lanzerotti, L. J.: 1986, *Nature* **323**, 694–696.
Milillo, A., and Orsini, S.: 2001, Energetic Neutral Atoms: Potential Merits and First Observations, *Recent Research Developments in Geophysical Research, Research Signpost* **3**, Trivandrum-India, 153.
Mitchell, D. G., Williams, D. J., Huang, C. Y., Frank, L. A., and Russell, C. T.: 1990, *Geophys. Res. Lett.* **17**, 583.
Moore, T. E., Chandler, M. O., Fok, M.-C., Giles, B. L., Delcourt, D. C., Horwitz, J. L. *et al.* : 2001, *Space Sci. Rev.* **95**, 555.
Morgan, T. H., and Killen, R. M.: 1997, *Planet Space. Sci.* **45**, 81–94.
Morgan, T. H., and Shemanski, D. E.: 1991, *J. Geophys. Res.* **96**, 1351–1367.
Morgan, T. H., Zook, H. A., and Potter, A. E.: 1988, *Icarus* **75**, 156–170.
Mura, A., Orsini, S., Milillo, A., Delcourt, D., Massetti, S., and De Angelis, E.: 2004, *Icarus*, accepted.
Mussett, A. E.: 1969, *Geophys J. Roy. Astron. Soc.* **18**, 257–303.
Ness, N. F., Behannon, K. W., Lepping, R. P., and Whang, Y. C.: 1975, *Nature* **255**, 204.
Ness, N. F., Behannon, K. W., and Lepping, R. P.: 1976, *Icarus* **28**, 479.
Ogilvie, K. W., Scudder, J. D., Vasyliunas, V. M., Hartle, R. E., and Siscoe, G. L.: 1977, *J. Geophys Res.* **82**, 1807–1824.

Onose, N., and Fujiwara, A.: 2003, Velocity distributions of fragments and its time dependence, *LPI Contribution* 1155, Houston, Texas, p 55.
Orsini, S., Milillo, A., De Angelis, E., Di Lellis, A. M., Zanza, V., and Livi, S.: 2001, *Planet. Space Sci.* **49,** 1659.
Orsini, S., and Milillo, A.: 1999, *Il Nuovo Cimento* **22**C, N 5, 633.
Paige, D. A., Wood, S. E., and Vasavada, A. R.: 1992, *Science* **258**, 643–646.
Palme, H.: 2000, *Space Sci. Rev.* **192**, 237–262.
Potter, A. E.: 1995, *Geophys. Res. Lett.* **22**, 3289–3292.
Potter, A. E., and Morgan, T. H.: 1985, *Science* **229**, 651–653.
Potter, A. E., and Morgan, T. H.: 1986, *Icarus* **67**, 336–340.
Potter, A. E., and Morgan, T. H.: 1987, *Icarus* **71**, 472–477.
Potter, A. E., and Morgan, T. H.: 1990, *Science* **248**, 835–838.
Potter, A. E., and Morgan, T. H.: 1997a, *Planet. Space. Sci.* **45**, 95–100.
Potter, A. E., and Morgan, T. H.: 1997b, *Adv. Space Res.* **19,** 1571–1576.
Potter, A. E., Killen, R. M., and Morgan, T. H.: 1999, *Plan. Space Sci.* **47**, 1441–1448.
Potter, A. E., Killen, R. M., and Morgan, T. H.: 2002a, *Meteorit. Planet. Sci.* **37**, 1165–1172.
Potter, A. E., Anderson, C. M., Killen, R. M., and Morgan, T. H.: 2002b, J. *Geophys. Res.* **107**(E6), 10.1029/2000JE001493.
Roelof, E. C.: 1987, *Geophys. Res. Lett.* **14**, 652.
Roelof, E. C., Mitchell, D. G., and Williams, D. J.: 1985, *J. Geophys. Res.* **90**, 10991.
Russell, C. T., Baker, D. N., and Slavin, J. A.: 1988, The magnetosphere of Mercury, in F. Vilas, C. R. Chapman, and M. S. Matthews (eds.), *Mercury,* Univ. of Arizona Press, Tucson, pp. 514–561.
Sackmann, I. J., and Boothroyd, A. I.: 2002, *Ap. J.* **583**, 1024–1039.
Salvail, J. R., and Fanale, F. P.: 1994, *Icarus* **111**, 441–455.
Sarantos, M., Reiff, P. H., Hill, T. W., Killen, R. M., and Urquhart, A. L.: 2001, *Planet. Space Sci.* **49**, 1629–1635.
Schubert, G., Ross, M. N., Stevenson, D. J., and Spohn, T.: 1988, Mercury's thermal history and the generation of its magnetic field, in F. Vilas, C. R. Chapman, and M. S. Matthews (eds.), Mercury, Univ. of Arizona Press, Tucson, p. 461.
Shemansky, D. E.: 1988, Revised atmospheric species abundances at Mercury: The debacle of bad *g* values, *Mercury Messenger 2, Lunar and Planet. Inst.,* Housten, Texas, U.S.A., p. 1.
Shemansky, D. E., and Broadfoot, A. L.: 1977, *Rev. Geophys.* **15**, 491–499.
Shemansky, D. E., and Morgan, T. H.: 1991, *Geophys. Res. Lett.* **18**, 1659–1662.
Siscoe, G. L., and Christofer, L.: 1975, *Geophys. Res. Lett.* **2**, 158.
Siscoe, G. L., Ness, N. F., and Yeates, C. M.: 1975, *J. Geophys Res.* **80**, 4359–4363.
Sieveka, E. M., and Johnson, R. E.: 1984, *Astrophys. J.* **287**, 418–426.
Simpson, J. A., Eraker, J. H., Lamport, J. E., and Walpole, P. H.: 1974, *Science* **185**, 160–166.
Slade, M. A., Butler, B. J., and Muhleman, D. O.: 1992, *Science* **258**, 635–640.
Slavin, J. S., and Holzer, R. E.: 1981, *J. Geophys Res.* **86**, No. 13, 11, 401–11, 418.
Slavin, J. A., Owen, J. C. J., Connerney, J. E. P., and Christen, S. P.: 1997, *Planet. Space Sci.* **45**, 133–141.
Smyth, W. H.: 1986, *Nature* **323**, 696–699.
Solomon, S. C., McNutt, R. L., Gold, R. E., Acuña, M. H., Baker, D. N., Boynton, W. V. *et al.* : 2001, *Plan. Space Sci.* **49**(14–15), 1445–1465.
Speiser, T. W.: 1965, *J. Geophys. Res.* **70**, 4219.
Sprague, A. L.: 1992, *J. Geophys. Res.* **97**, 18257–18264.
Sprague, A. L., Kozlowski, R. W. H., and Hunten, D. M.: 1990, *Science* **249**, 1140–1143.
Sprague, A. L., Kozlowski, R. W. H., and Hunten, D. M.: 1993, *Icarus* **104**, 33–37.
Sprague, A. L., Hunten, D. M., and Lodders, K.: 1995, *Icarus* **118**, 211–215.
Sprague, A. L., Hunten, D. M., and Lodders, K.: 1996a, *Icarus* **123**, 247.

Sprague, A. L., Hunten, D. M., and Grosse, F. A.: 1996b, *Icarus* **123**, 345–349.
Sprague, A. L., Kozlowski, R. W. H., Hunten, D. M., Schneider, N. M., Domingue, D. L., Wells, W. K. *et al.*: 1997, *Icarus* **129**, 506–527.
Starukhina, L. V.: 2000, *LPSC* **31**, 1301.
Stebbings, R. F., Smith, C. H., and Ehrahardt, H.: 1964, *J. Geophys. Res.* **69**, 2349.
Strom, R. G.: 1984, Mercury, in M. H. Carr (ed.), *The Geology of the Terrestrial Planets,* NASA Sp. **469**, Washington, D.C., pp. 13–55.
Sugita, S., Schultz, P. H., and Adams, M. A.: 1997, *Lunar Planet. Sci. Conf. 28th*, 1393–1394.
Tonks, W. B., Melosh, H. J., and McKinnon, W. B.: 1990, *LPSC* **21**, 1260–1261.
Vilas, F.: 1985, *Icarus* **64**, 503.
Weidenschilling, J.: 1978, *Icarus* **35**, 99–111.
Weidenschilling, S. J., Spaute, D., Davis, D. R., Marzari, F., and Ohtsuki, K.: 1997, *Icarus* **128**(2), 429–455.
Wetherill, G. W., and Chapman, C. R.: 1988, Asteroids and meteorites, in J. F. Kerridge and M. S. Matthews (eds.), *Meteorites and the Early Solar System,* Univ. of Arizona Press, Tucson, pp. 35–67.
Wetherill, G. W., and Stewart, G. R.: 1989, *Icarus* **77**, 330–357.
Wiens, R. C., Burnett, D. S., Calaway, W. F., Hansen, C. S., Lykkem, K. R., and Pellin, M. L.: 1997, *Icarus* **128**, 386–397.
Wurz, P., and Blomberg, L.: 2001, *Plan. Space Sci.* **49**, 1643–1653.
Wurz, P., and Lammer, H.: 2003, *Icarus* **164**(1), 1–13.
Yakshinskiy, B. V., and Madey, T. E.: 1999, *Nature* **400**, 642–644.
Yakshinskiy, B. V., and Madey, T. E.: 2000, *Surface Science* **451**, 160–165.